



Frictional properties of simulated anhydrite-dolomite fault gouge and implications for seismogenic potential



A.M.H. Pluymakers^{*},¹, A.R. Niemeijer, C.J. Spiers

HPT Laboratory, Faculty of Geosciences, Utrecht University, Budapestlaan 4, 3584 CD, Utrecht, The Netherlands

ARTICLE INFO

Article history:

Received 19 August 2015

Received in revised form

11 November 2015

Accepted 16 November 2015

Available online 13 January 2016

Keywords:

Earthquake nucleation

CO₂ storage

Italian Apennines

Evaporites

Fault stability

Induced seismicity

ABSTRACT

The frictional properties of anhydrite-dolomite fault gouges, and the effects of CO₂ upon them, are of key importance in assessing the risks associated with CO₂ storage in reservoir formations capped by anhydrite-dolomite sequences, and in understanding seismicity occurring in such formations (such as the Italian Apennines). Therefore, we performed velocity-stepping direct-shear experiments on simulated dolomite, anhydrite and 50:50 anhydrite/dolomite gouges, at representative in-situ conditions (120 °C and $\sigma_n^0 = 25$ MPa). They were conducted under vacuum, or else using water or CO₂-saturated water as pore fluid ($P_f = 15$ MPa). Friction coefficients varied between 0.55 and 0.7. All dry samples exhibited velocity-weakening behavior, whereas all wet samples exhibited velocity-strengthening behavior, without or with CO₂. This is consistent with trends previously reported for such gouges. A compilation of literature data shows that the transition from velocity-strengthening to velocity-weakening occurs in these materials between 80 and 120 °C when dry, and between 100 and 150 °C when wet. This implies little seismogenic potential for wet dolomite, anhydrite and mixed gouges under CO₂ storage conditions at 2–4 km depth. Seismic slip in the Italian Apennines at depths of ~6 km and beyond may be explained by the velocity-weakening behavior expected in anhydrite and especially dolomite at temperatures above 150 °C.

© 2016 Elsevier Ltd. All rights reserved.

1. Introduction

Many hydrocarbon fields are capped by evaporites, the base of which often contains tens or even hundreds of meters of interbedded anhydrite and dolomite (respectively CaSO₄ and (Ca,Mg) CO₃). Such thick layers are usually deposited in a deep basin setting, and examples include the Zechstein sequence that overlies many of the Rotliegend gas fields in the Netherlands and North Sea area (Geluk, 2000, 2007), the Sudair Formation overlying many of the Qatar gas fields (Alsharhan and Nairn, 1994; Bai and Xu, 2014), and the Midale and Muskeg Formations, that overlie respectively the Weyburn and the Zama oil fields in Canada (Smith et al., 2011; Bennion and Bachu, 2013). Once depleted, the hydrocarbon reservoirs offer attractive options for CO₂ storage. To ensure safe and effective CO₂ storage, it is important to evaluate the geomechanical

stability of faults that crosscut the caprock. Such faults are known to be preferential leakage pathways in natural reservoirs (Miočic et al., 2013) and when cross-cutting an anhydrite caprock, they will generally contain anhydrite-rich fault gouges, with variable amounts of dolomite. A thorough understanding of the frictional properties not only of anhydrite but also of dolomite and mixed fault gouges is therefore needed, as well as knowledge of any possible effects of CO₂-bearing fluids. Such data is also relevant to understanding natural seismicity in tectonically active regions dominated by carbonate/anhydrite evaporite formations, of which the Italian Apennines are a well-studied example. There, the M-6 Colfiorito sequence (1997–1998) and the destructive M-6 L'Aquila earthquake (2009) nucleated in respectively the interbedded anhydrite/dolomite formation (Mirabella et al., 2008; Collettini et al., 2009) and a thick dolomite sequence (Speranza and Minelli, 2014), with nucleation depths lying between 5 and 10 km. Moreover, this region is characterized by major CO₂ degassing from deeper levels (e.g. Chiodini et al., 1999; Collettini et al., 2008; Improta et al., 2014), so that data on the effects of CO₂-bearing fluids on the frictional properties of carbonate/anhydrite fault rocks are also directly relevant here.

^{*} Corresponding author. Physics of Geological Processes, University of Oslo, Postboks 1048, Blindern, 0316 Oslo, Norway.

E-mail addresses: a.m.h.pluymakers@fys.uio.no (A.M.H. Pluymakers), A.R.Niemeijer@uu.nl (A.R. Niemeijer), C.J.Spiers@uu.nl (C.J. Spiers).

¹ Now at Physics of Geological Processes, University of Oslo, Oslo, Norway.

One of the mechanisms by which a fault can generate an earthquake lies in its capacity to weaken as motion accelerates, via “velocity-weakening behavior”. Even without velocity weakening, marked slip weakening, i.e. weakening with increasing displacement, can also lead to accelerating slip and hence seismogenesis (c.f. Ikari et al., 2013; Ohnaka, 2013). On the other hand, if a fault becomes stronger with increasing slip and/or increasing slip velocity (e.g. via “velocity-strengthening” behavior), it is not capable of generating accelerating slip. In the current paper we will focus on the velocity dependence of friction. This is classically described by the rate-and-state friction (RSF) equations (Dieterich, 1978, 1979; Ruina, 1983), which have been successful in describing and explaining natural seismicity (Sone and Shimamoto, 2009; Barbot et al., 2012; Noda and Lapusta, 2013; den Hartog and Spiers, 2014; Niemeijer and Vissers, 2014). The Dieterich-type RSF equation describes fault strength evolution upon a velocity step as follows:

$$\mu = \mu_0 + a \ln\left(\frac{V}{V_0}\right) + b \ln\left(\frac{V_0 \theta}{d_c}\right), \quad \text{with} \quad \frac{d\theta}{dt} = 1 - \frac{V\theta}{d_c}. \quad (1)$$

Which at steady state reduces to:

$$(a - b) = \frac{\Delta\mu}{\ln(V/V_0)} \quad (2)$$

Here μ_0 and μ are the friction coefficients measured before and after individual velocity steps, V_0 and V represent the sliding velocities imposed before and after each step, a represents the magnitude of the direct effect of changing velocity on the friction coefficient μ , b represents the subsequent evolution of μ , θ is a state variable (generally interpreted as reflecting the average lifetime of load supporting contact points or asperities), and d_c is the slip distance necessary to establish a new steady state strength and internal structure (i.e. to renew the population of load supporting contact points). Positive values of $(a-b)$ describe velocity-strengthening behavior, whereas negative values of $(a-b)$ describe velocity-weakening behavior.

In contrast to quartz and clay, carbonates like dolomite and calcite, and sulphates, like anhydrite, are ionic solids, characterized by a crystal structure displaying distinctive brittle cleavage properties (e.g. Johnsen, 2004) and similar indentation and Mohs hardness (e.g. Mohs, 1820; Taylor, 1949; Tabor, 1956, 1970; Johnsen, 2004). They also show a transition from brittle to plastic behavior at relatively low temperatures compared to silicates (from cataclasis to pressure solution, twinning and dislocation glide, see Müller and Siemes, 1974; Rutter, 1974; Wenk and Shore, 1975; Barber et al., 1981; Müller et al., 1981; Schmid et al., 1987; Dell'Angelo and Olgaard, 1995; Bruhn et al., 1999; Davis et al., 2008; Delle Piane et al., 2008) and they show a decrease in solubility with increasing temperature (e.g. Langmuir, 1997). Additionally, through their relatively high solubility at low temperatures, they are prone to deformation by fluid-assisted diffusive processes such as pressure solution. Indeed, pressure solution has been shown to be an important deformation mechanism in both anhydrite (Pluymakers and Spiers, 2015; Pluymakers et al., 2014a) and calcite aggregates (Zhang and Spiers, 2005; Zhang et al., 2010) under upper crustal conditions.

On this basis, carbonate and anhydrite fault gouge can be expected to show similarities in their frictional behavior at upper crustal conditions, while differing significantly from silicate gouges at similar pressures and temperature. Previous work on the velocity-dependence of friction in wet anhydrite gouges, at P-T conditions relevant to CO₂ storage, has demonstrated velocity-strengthening behavior, both without and with supercritical CO₂ (Pluymakers et al., 2014b; Pluymakers and Niemeijer, 2015).

However, limited data recorded by Scuderi et al. (2013), on 50:50wt % mixtures of anhydrite and dolomite tested wet at 75 °C, suggests that $(a-b)$ may decrease compared to the end-member compositions, and may produce velocity-weakening (Scuderi et al., 2013). If $(a-b)$ decreases in mixed anhydrite-dolomite gouges such that marked velocity-weakening behavior occurs under CO₂ storage conditions, this may have important consequences with respect to induced seismicity and risk assessment. Data on the frictional behavior of mixed anhydrite-dolomite fault gouges under upper crustal pressure and temperature conditions are very few, despite intimate mixing inferred from field and borehole studies (e.g. De Paola et al., 2008; Collettini et al., 2009; Trippetta et al., 2013; Hangx et al., 2014), and no published data exist on how the friction of dolomite and dolomite/anhydrite aggregates is affected by the presence of CO₂-bearing fluids.

To fill this knowledge gap, we have performed direct-shear experiments on simulated gouges of anhydrite, dolomite and on 50:50wt% anhydrite/dolomite mixtures. The experiments were performed at a temperature of 120 °C and an effective normal stress of 25 MPa with the pore fluid system under vacuum (dry testing conditions) or else pressurized with water or with CO₂-saturated water. These conditions were chosen to be as close as possible to those expected in anhydrite/dolomite-capped CO₂ storage reservoirs at 2–4 km depth (assuming hydrostatic pore fluid pressure), as well as to natural seismicity in the Italian Apennines (Mirabella et al., 2008; Collettini et al., 2009). The expected in-situ normal stresses may be as low as 20 MPa due to the high fluid pressures, up to 85% of lithostatic pressure (Collettini et al., 2009; Trippetta et al., 2013). To investigate the robustness of our findings for a wider, more realistic range of conditions relevant to CO₂ storage and to seismicity in the Apennines, we compare our results with previous data on the frictional properties of dolomite and anhydrite at a range of different pressure and temperature conditions.

2. Experimental methods

We conducted velocity-stepping, direct shear experiments on simulated fault gouges consisting of crushed dolomite (labeled D in all figures and in Table 1), of crushed anhydrite (labeled A) or of a 50:50wt% mixture (labeled 50:50). Runs were performed dry, with the pore fluid system under vacuum (labeled dry or VAC), or with the pore fluid system pressurized with water (labeled wet or W), or using pre-wetted samples pressurized with supercritical CO₂ (labeled wet + CO₂ or WC). The temperature used in all experiments was 120 °C, and the effective normal stress (σ_n^e) was 25 MPa. When using a pore fluid phase, its pressure was 15 MPa. All experiments and corresponding conditions are listed in Table 1.

The dolomite gouge used was prepared by crushing cleaved single crystals from Butte, Montana, obtained commercially through Ward's Natural Science. Anhydrite gouge was prepared by crushing core material retrieved from a borehole in Overijssel, the Netherlands (courtesy of Shell Global Solutions), where it was taken from the Permian Zechstein 1 Anhydrite Member, at 2–3 km depth (see for a detailed description Hangx et al., 2014). After crushing, the powders were sieved to obtain simulated end-member gouges with a grain size smaller than 50 µm. Laser particle size analyses indicated a similar initial maximum grain size of 50 µm and a mode grain size of ~32 µm for all samples. The sieved powders were further analyzed using ThermoGravimetric Analysis (TGA) and/or X-Ray-Diffraction (XRD), which confirmed the anhydrite gouge to be > 95 wt% anhydrite with trace amounts of dolomite. The dolomite gouge consisted of >90 wt% dolomite with trace amounts of calcite, albite and quartz. For the experiments on the 50:50 wt% mixtures, we mixed a single batch of 8 g of the anhydrite with 8 g of the dolomite powder.

Table 1
Conditions of all experiments plus key data.

	FT	T [°C]	σ_n [MPa]	P_f [MPa]	h_0 [mm]	h_f [mm]	mass [g]	ϕ_0 [-]	ϕ_f [-]	μ_{2mm} [-]	$\mu_{4.8mm}$ [-]
<i>dolomite samples</i>											
VAC100D2	VAC	120	25	—	1.44	1.12	3.99	0.43	0.18	0.629	0.578
W100D1	W	120	40	15	1.37	1.47	3.97	0.40	—	0.611	0.584
WC100D1	CW	120	40	15	1.34	1.10	4	0.39	0.16	0.588	0.556
<i>50:50 anhydrite/dolomite samples</i>											
VAC5050-1	VAC	120	25	—	1.40	1.10	3.99	0.42	0.16	0.634	0.607
VAC5050-2	VAC	120	25	—	1.40	1.12	3.94	0.42	0.19	0.610	0.618
W5050-1	W	120	40	15	1.52	1.00	3.97	0.46	0.09	0.635	0.551
WC5050-1	CW	120	40	15	1.27	1.12	3.99	0.35	0.18	0.604	0.562
<i>anhydrite samples</i>											
VAC100A1	VAC	120	25	—	1.40	1.20	4	0.41	0.23	0.684	0.681
VAC100A2	VAC	120	25	—	1.50	1.15	4	0.45	0.20	0.708	0.658
W100A1	W	120	40	15	1.80	1.10	4	0.54	0.16	0.572	0.473
WC100A1	CW	120	40	15	1.16	0.61	2.5	0.56	0.05	0.547	0.490

The (a–b) values for half of the sequence of the dry and wet anhydrite end-member experiments were reported previously by Pluymakers and Niemeijer (2015) and the wet + CO₂ experiments were reported by Pluymakers et al. (2014b). FT represents fluid type, T temperature, σ_n the applied normal stress, P_f the fluid pressure, h_0 initial gouge sample layer thickness, h_f final layer thickness, ϕ_0 is the porosity before emplacement of the sample assembly in the pressure vessel, ϕ_f is the final porosity after depressurization, cooling and extraction of the assembly calculated from final sample thickness, μ_{2mm} the friction coefficient measured at a displacement of 2 mm and $\mu_{4.8mm}$ that at a displacement of 4.8 mm. In addition, VAC denotes vacuum-dry samples, W wet samples (no CO₂), and CW samples containing CO₂-saturated water.

The experiments were performed using a direct shear testing assembly mounted in a constant-velocity triaxial testing machine (Fig. 1a), allowing sliding velocity to be stepped near-instantaneously using a manually operated motor/gear-box/ball-screw system. Confining pressure (hence normal stress) was kept constant using a lab-built, servo-controlled syringe pump. When using water only as a pore fluid, the pressure in the pore fluid system was measured using a Jenssen pressure transducer (50 MPa range; resolution ± 0.02 MPa) and maintained constant using another servo-controlled syringe pump. When using CO₂-saturated water, pore pressure was applied to the water-saturated sample assembly by pressurizing with CO₂, keeping the pressure constant using an ISCO 65D pump, with a built-in Honeywell transducer

allowing pressure measurement and control (150 MPa range; pressure resolution ± 0.00138 MPa). For more details on the triaxial machine and pore fluid control system we refer to Hangx et al. (2010a).

Samples consisted of a layer of simulated gouge sandwiched in the direct shear assembly shown in Fig. 1b (for a detailed description see Samuelson and Spiers, 2012). The layer was pre-pressed onto one of the direct shear driver blocks by distributing and compacting 4 g of simulated gouge in a specially designed jig, leading to a layer thickness of 1.24 ± 0.23 mm, and a length and width of 47 mm and 35 mm respectively. Once assembled, with silicone polymer filler plugs in place, the direct shear set formed a smooth cylinder that could be jacketed easily, first with fluorinated

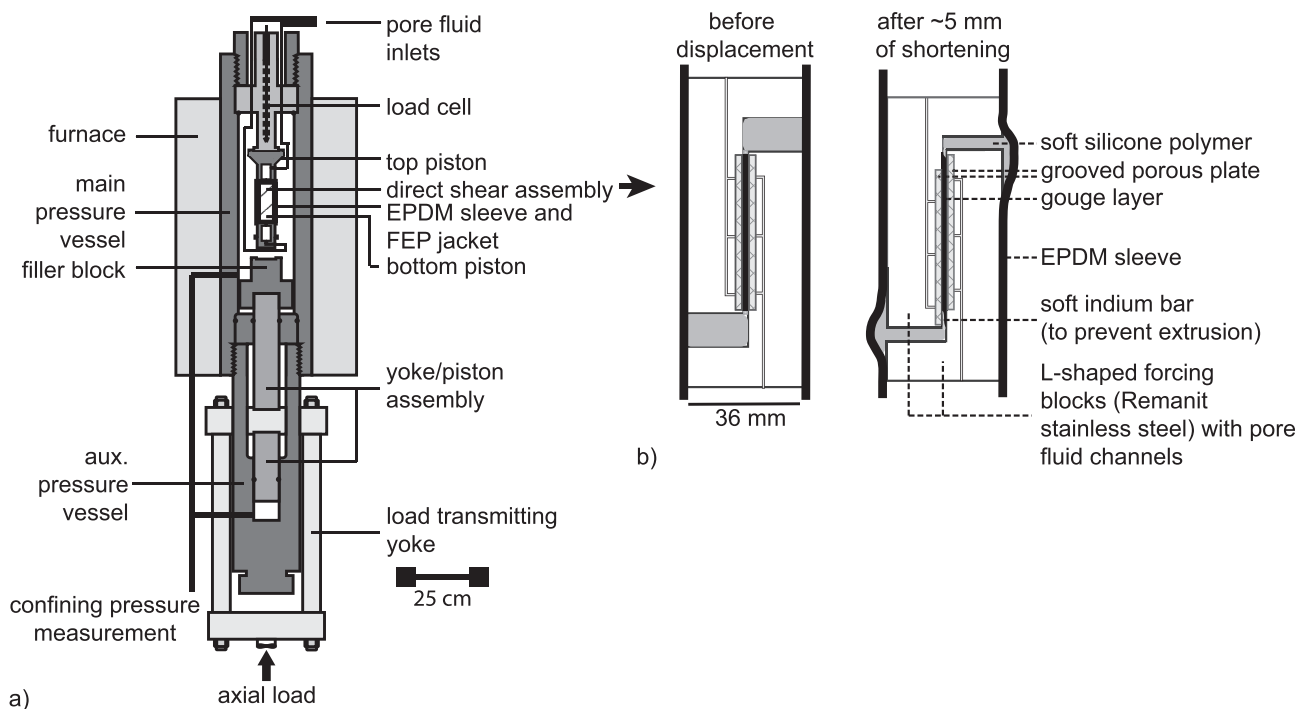


Fig. 1. Schematic diagram of a) the triaxial testing apparatus (from Hangx et al., 2010a, 2010b) and b) the direct shear assembly used in this study. The direct shear assembly is drawn before (left) and after shearing the sample by ~5 mm displacement (right).

ethylene propylene (FEP) heat-shrink tube and then an ethylene propylene diene monomer (EPDM) rubber sleeve. The latter was sealed against the two direct shear driver blocks using wire tourniquets. For the experiments performed using CO₂-saturated water as pore fluid, the assembly was then placed in a water bath, and water was drawn in under a vacuum. The dry or wet assembly was subsequently emplaced in the pressure vessel and brought to the target confining pressure, fluid pressure, and temperature. In the wet-only experiments, fluid pressure was applied using deionized water in the pore fluid system. Due to the fine-grained nature of the samples combined with the small fluid volume present inside the sample pores and the 4–5 h needed to achieve stable pressure and temperature, it is assumed that local chemical equilibrium is approached before initiating each experiment (c.f. Pluymakers and Niemeijer, 2015). In experiments performed using CO₂-saturated pore water, CO₂ pressure was applied to the pre-wetted samples, whereas for dry samples the pore fluid system was continuously attached to a vacuum pump during heating, pressurization of the confining pressure and testing. Once pressure and temperature were stable, the loading ram was brought into contact with the sample at a velocity of 5 $\mu\text{m s}^{-1}$. Velocity steps were then applied to shear the sample, cycling through the sequence 5.3 \rightarrow 0.21 \rightarrow 1.1 \rightarrow 11 \rightarrow 0.21 $\mu\text{m s}^{-1}$, employing 2–0.4–0.7–0.7–0.7 mm displacement intervals. After completing this sequence, the piston was retracted at 2.2 $\mu\text{m s}^{-1}$ until the sample was fully unloaded. The piston was then retracted further at 22 $\mu\text{m s}^{-1}$, followed by depressurization of the pore fluid and oil pressure systems, and then by cooling and extraction of the sample assembly. Following extraction, the sample assembly was opened and fragments of the gouge are salvaged where possible. Part of the sample was disaggregated and analyzed using a laser particle sizer. After impregnation with epoxy, the salvaged fragments were cut into thick sections, which were polished for subsequent microstructural analysis with a scanning electron microscope (SEM). A porosity estimate was made from the SEM images obtained, using a point counting method with a random grid using JMicrovision image analysis software. For each sample 500 points were taken on the low magnification micrographs (50x to 75x) and categorized as porosity, grains, dilated cracks/shear bands or unidentifiable points (the evolution of the count with number of points counted is shown in Appendix A1).

Internal axial load, piston displacement, confining pressure, temperature, pore fluid pressure (water and CO₂) and pore fluid volume change signals were logged at a frequency of 5 Hz, using a 16-bit National Instruments A/D converter and VI-Logger software. The raw data were processed to obtain shear strength τ (MPa), effective normal stress σ_n^e (MPa) and friction coefficient μ (–), defined $\mu = \tau/\sigma_n^e$ and hence ignoring cohesion, versus time and displacement. To obtain shear displacement (mm) we corrected all displacement data for apparatus distortion using pre-determined polynomial stiffness calibrations. Displacement strengthening or weakening rates are obtained from a linear fit to the friction coefficient versus time in each displacement interval once steady state was reached. These fits were normalized to velocity to obtain the rate as $\Delta\mu/\Delta x$ (mm^{-1}).

The velocity dependence of friction was analyzed using the Dieterich-type evolution RSF equation (“slowness law”) (Dieterich, 1978, 1979). The evolution of friction upon a change in load-point velocity from V_0 to V can be calculated using equation (1), coupled with an equation describing the dynamic interaction with the elastic loading frame of the testing system (c.f. Reinen and Weeks, 1993; Saffer and Marone, 2003). To obtain values for the RSF parameters in (1), we used the inversion technique described elsewhere (e.g. by Reinen and Weeks, 1993; Saffer and Marone, 2003). An example fit is shown in Fig. 2. We do not report d_c

values however, since inversions typically showed large uncertainties in this parameter. These were attributed to the use of the manually operated gear-box, where switching gears takes ½ second or less. This change of gears always takes slightly different amounts of time and encompasses different “apparent” displacements. Since the RSF parameters a and b are insensitive to the time over which a velocity-change is imposed, the use of a manual gearbox should not affect the values obtained for these parameters. The delay in the velocity-step is modeled using an artificially low stiffness, which led to sensible model fits to the data (Fig. 2, Appendix Table A2). For selected experiments we also calculated $(a-b)$ using the steady state method (c.f. Pluymakers et al., 2014b), which led to similar results for $(a-b)$. Fitting the Ruina evolution equation (Ruina, 1983) instead of the Dieterich equation resulted in practically indistinguishable values for a and b (Appendix Table A2 for the values plus their errors).

3. Results

3.1. Dry experiments

The results for vacuum-dry experiments show that the shear stress supported increases rapidly in the first millimeter of displacement, in a similar manner for all compositions (Fig. 2a). Macroscopic yield occurs at a displacement of approximately 1 mm, followed by a broad maximum in strength and mostly fairly minor but continuous slip weakening beyond about 2 mm displacement. Pure anhydrite samples are the strongest, showing near-peak friction coefficients, measured at 2 mm displacement, of $\mu_{2\text{mm}} = 0.684$ and $\mu_{2\text{mm}} = 0.708$, which is slightly higher than the similar values obtained for dolomite ($\mu_{2\text{mm}} = 0.629$) and the 50:50 mixture, ($\mu_{2\text{mm}} = 0.610$ and $\mu_{2\text{mm}} = 0.634$) – see Figs. 2a and 3a and Table 1. The rate of post-peak displacement-weakening shows a similar spread for the three compositions tested dry (Fig. 2a, Table 1), and values tend to increase with decreasing sliding velocity (Fig. 4a).

All dry samples exhibit both positive and negative $(a-b)$ values, with negative values, i.e. velocity-weakening behavior, occurring mainly at the lowest velocities investigated (0.21 and 1.1 $\mu\text{m s}^{-1}$, see Fig. 5a). Stick-slip behavior occurs during all of these low velocity intervals in the dry anhydrite and dolomite samples (Fig. 2a), whereas the 50:50 mixtures exhibit stick-slip only during the 0.21 $\mu\text{m s}^{-1}$ interval at the highest displacements reached (Fig. 2a). The range of $(a-b)$ values obtained for each composition is shown in Fig. 5a and is widest for the anhydrite gouge ($-0.0081 < (a-b) < 0.0027$), followed by the 50:50 mixtures ($-0.0019 < (a-b) < 0.0015$) and then the pure dolomite samples ($-0.0017 < (a-b) < 0.0007$). Ignoring the single strongly negative $(a-b)$ value obtained for anhydrite gouge at 1.1 $\mu\text{m s}^{-1}$, $(a-b)$ values increase with increasing velocity in a similar manner for all three gouge types (Fig. 6a). Individual values of a and b are strongly variable, with no clear trends with velocity or composition, so were accordingly not plotted.

3.2. Wet experiments

All wet-tested samples show a similar evolution of shear stress with displacement to that observed for the dry samples. All show displacement weakening at displacements beyond 2.5 mm (Fig. 2b). Wet anhydrite samples exhibit the lowest friction coefficient ($\mu_{2\text{mm}} = 0.572$) at a displacement of 2 mm compared to dolomite and the 50:50 mixture, which show similar values of 0.611 and 0.635 respectively (Figs. 2b and 3a, Table 1). Hence, the wet anhydrite samples are weaker than the dry equivalents, but for dolomite and the 50:50 mixtures the strength is similar both dry and wet. At the intermediate and highest velocity, dolomite samples exhibit the least displacement weakening (Fig. 4b). The trends

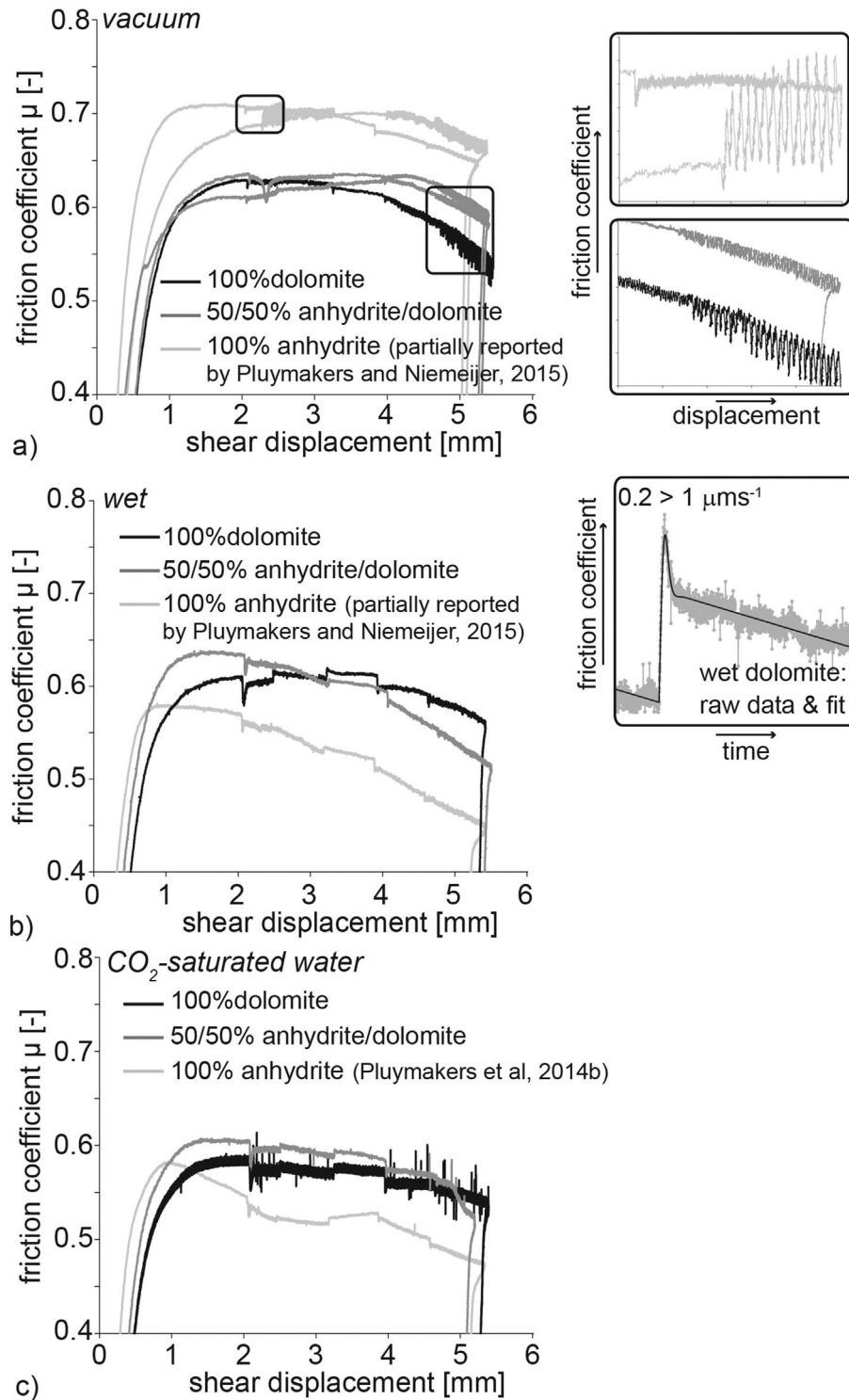


Fig. 2. Frictional strength versus shear displacement. a) vacuum-dry samples. Insets (right) show blow-up of friction coefficient vs. displacement curve, clearly showing the stick-slip events. b) wet samples. Inset (right) shows blow-up of friction coefficient vs. displacement curve for wet dolomite at the first velocity step (2 mm). Superimposed in black is an example fit of the RSF inversion of this step. c) wet + CO_2 samples. The oscillations seen in the 100% dolomite curve in c) are related to problems with the pump controlling the CO_2 pressure.

with velocity are similar as observed in the dry samples (see Fig. 4b).

Regarding velocity dependence, all wet samples exhibit velocity-strengthening behavior. Dolomite shows a range of (a - b) values between 0.0025 and 0.0060, anhydrite between 0.0020 and 0.0040, and the 50:50 mixture between 0.00050 and 0.0035

(Fig. 5b). The mixture thus shows slightly less marked velocity-strengthening than either end-member. At the intermediate sliding velocity of $1.1 \mu\text{ms}^{-1}$, (a - b) values show a maximum for all three compositions (Fig. 6b). The separate a - and b -values again vary considerably without any clear trends and are thus not presented.

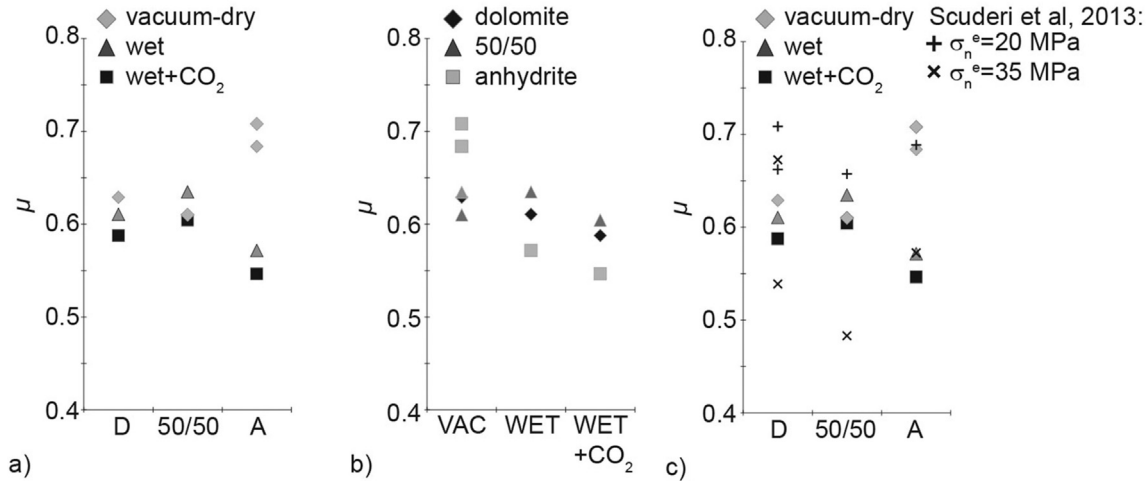


Fig. 3. Frictional strength, measured at 2 mm displacement versus a) gouge composition and b) fluid type. c) Frictional strength versus gouge composition measured at 2 mm displacement in the current study, plus the corresponding values obtained by Scuderi et al. (2013) (wet only). D = dolomite samples, A = anhydrite samples, 50:50 = dolomite/anhydrite mixture, VAC = vacuum-dry samples, WET = wet samples (no CO₂), WET + CO₂ = samples containing CO₂-saturated water.

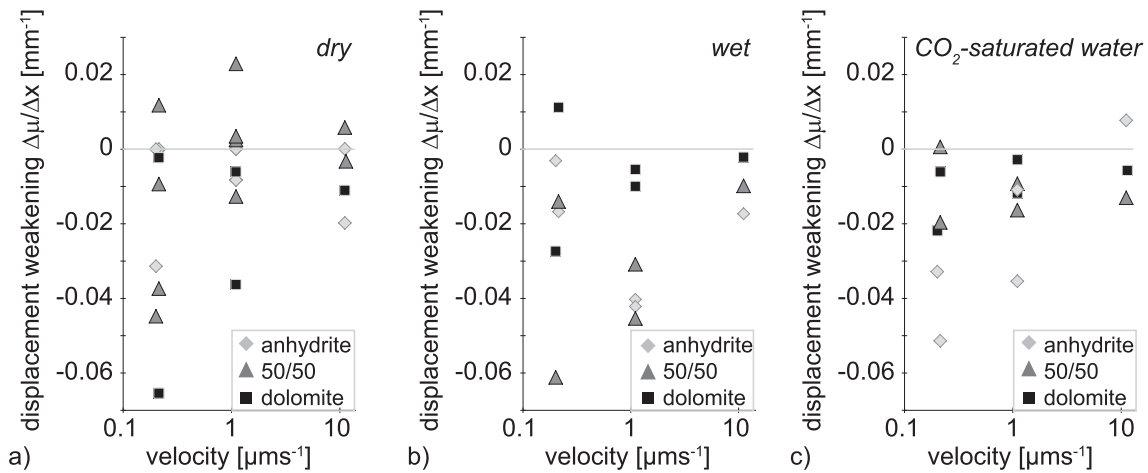


Fig. 4. Displacement weakening rate versus velocity for a) vacuum-dry samples, b) wet samples, and c) wet + CO₂ samples. Note that displacement weakening was measured as the slope of a graph of μ versus x during intervals in which the velocity as indicated on the x-axis was imposed.

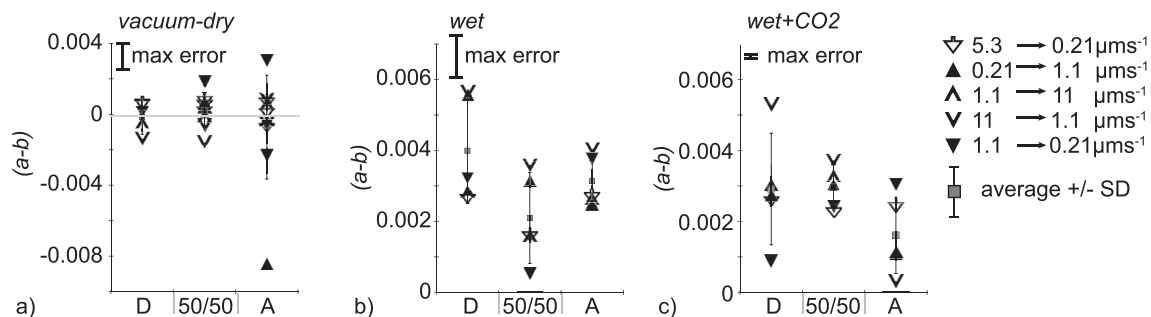


Fig. 5. Data on $(a-b)$ versus gouge composition for the different pore fluids used. The different symbols used to indicate the velocity-steps are listed to the right. Average values of $(a-b)$ are indicated in grey. The magnitude of the error in $(a-b)$ data is shown below the legend symbols (average ± 1 standard deviation). a) Samples tested under vacuum. b) Wet-tested samples. c) Samples tested with CO₂-saturated water.

3.3. Wet + CO₂ experiments

All samples tested with CO₂-saturated pore fluid (Table 1) show an evolution of shear strength with displacement that is again similar to the dry and wet experiments (Fig. 2, note that the

oscillations in c) are caused by problems in the pump controlling CO₂ pressure). The samples tested wet with CO₂ show displacement weakening from a displacement between 0.92 and 2.1 mm onwards. For all gouge compositions the friction coefficient μ_{2mm} for wet + CO₂ samples is 3–5% lower than for wet tested samples

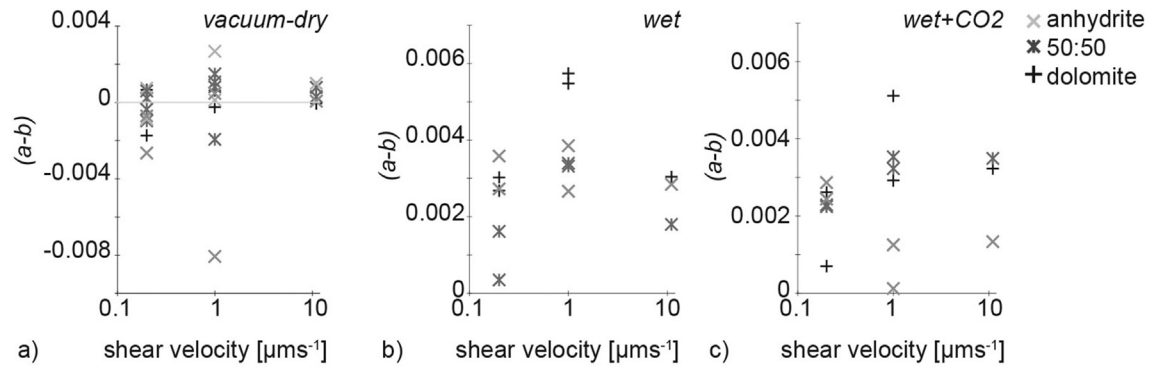


Fig. 6. Data on $(a-b)$ versus shear velocity [μms⁻¹] for the different pore fluids used in this study. Symbols are explained in the legend to the right. a) Samples tested under vacuum. b) Wet-tested samples. c) Samples tested with CO₂-saturated water.

without CO₂, i.e. only just above experimental variability (Table 1, Fig. 3). As for the wet tested samples, though, anhydrite is still the weakest of the three compositions ($\mu_{2mm} = 0.547$), while the values for dolomite and the 50:50 mixture are similar (0.605 and 0.588, respectively). With respect to displacement weakening, the wet + CO₂ samples exhibit similar trends to the wet samples (Fig. 4c).

Turning to the velocity-dependence, just like wet samples, samples tested wet with CO₂ exhibit velocity-strengthening behavior only, without any systematic differences between the end-member samples and the mixed sample. For all three compositions, an increase in velocity leads to an increase in $(a-b)$ (Fig. 6c). The separate a - and b -values obtained by inversion again show no clear trends with changing velocity or displacement.

3.4. Microstructural observations

Grain size analysis of dry and wet samples after testing with a laser particle sizer showed a similar change in grain size compared to the starting material, with an increase in sub-micron sized particles, and a widened distribution. Peak grain sizes after testing were 20–40 μm, mode grain size was 10–20 μm. The grain size distributions obtained are shown in Fig. 7.

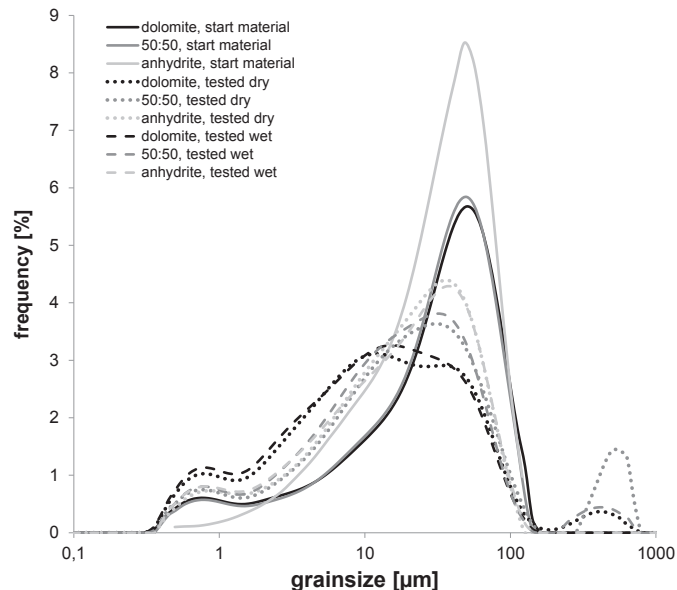


Fig. 7. Laser particle sizer data of the different gouge samples, before and after testing.

Impressions of the grooves present in the forcing-block/sample interfaces were absent in all of the experiments (Fig. 1b), indicating that the upper and lower surfaces of the gouge samples were lost during sample disassembly. Dolomite gouge samples were recovered but the sections that could be prepared from them were of insufficient quality to make reliable detailed observations. They showed roughly similar features as the anhydrite and the mixed gouges, which we will report here using the shear band terminology of Logan et al. (1979). Differences in porosity obtained from the microstructure and the one calculated from final sample thickness (Table 1) can be attributed to impregnation and thin section preparation.

Imaged using electron backscatter mode in the SEM, the dry tested 50:50 gouge shows the highest porosity. The point count indicated 39% porosity, 45% grains, 15% dilated cracks/shear bands and 2% unidentifiable points. The few dilated sample-sized cracks are aligned in a direction consistent with R1 Riedel shear bands (Fig. 8a). At the boundaries of these cracks we observe patchy zones of grain size reduction. The overall grain size of this sample is significantly lower than the sieve size of 50 μm used to prepare the starting gouges, with an abundance of grains of 10 μm and smaller (see Fig. 8b). Grain contacts are sharp, and most grains are angular and contain intragranular and transgranular cracks (Fig. 8b). The point count in the wet-tested mixed sample indicated 26% porosity, 61% grains, 7% dilated cracks/shear bands and 1% unidentifiable points (Fig. 8c, d, e). Dilated cracks in the R1 orientation are present here as well (Fig. 8c), surrounded by an up to 20 μm wide zone of reduced grain size (Fig. 8d). At the margins of the sample, patchy zones with intense grain size reduction are visible (Fig. 8e), implying that a Y shear was present but not fully preserved. Outside these localized zones of grain size reduction, the grain size and grain size distribution appears similar to that found in the body of the dry sample. Where visible, grain contacts are relatively flat in the wet sample, compared to the dry mixed sample. Again, most grains contain intragranular and transgranular cracks (Fig. 8d).

The dry-tested anhydrite sample studied using SEM is characterized by 30% porosity, 57% grains, 12% dilated cracks/shear bands and 1% unidentifiable points. En echelon R1 shear zones with intense internal grain size reduction (Fig. 8f–h) are present, as well as dilated cracks aligned in the R1 direction. The grain size outside these localized zones is variable, but overall the grain size is larger than in the dry mixed sample (Fig. 8h) and closer to the sieve size of 50 μm used in sample preparation. Grain contacts are sharp and most grains are angular. Most grains contain intragranular and transgranular cracks, but they appear less damaged than in the dry mixed sample. The point count for the wet-tested anhydrite sample indicated 29% porosity, 55% grains, 8% dilated cracks/shear bands

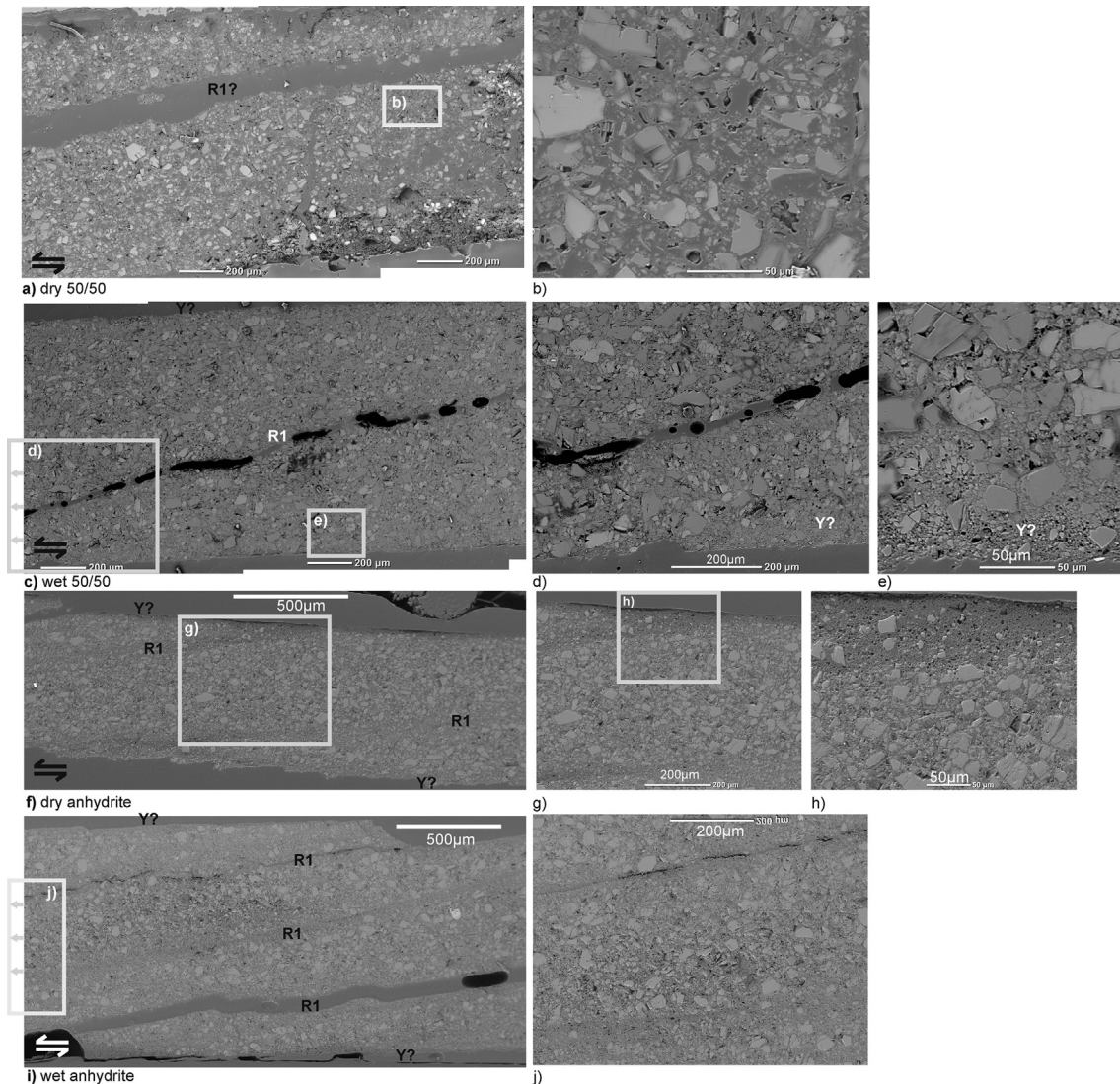


Fig. 8. Electron backscatter images of the microstructure displayed by 50:50 anhydrite/dolomite samples and by the anhydrite samples after velocity-steps tests at 120 °C. a&b) Mixed gouge sample, tested dry (coded VAC5050-2). A high-resolution version of this slide for use with the Virtual Microscope is available as eSlide: VM02080. c-e) Mixed gouge sample, tested wet (coded W5050-1). A high-resolution version of this slide for use with the Virtual Microscope is available as eSlide: VM02081. f-h) Pure anhydrite sample, tested dry (coded VAC100A2). A high-resolution version of this slide for use with the Virtual Microscope is available as eSlide: VM02082. i-j) Pure anhydrite sample, tested wet (coded W100A1). A high-resolution version of this slide for use with the Virtual Microscope is available as eSlide: VM02083.

and 8% unidentifiable points. It shows up to 50 μm wide, closely spaced *en echelon* R1 shear zones, about half of which are dilated by late fracturing of the sample (Fig. 8i). As in the dry-tested anhydrite sample, the wet-tested equivalent contains localized patches of intense grain size reduction scattered along the boundary of the sample, implying the likely presence of Y-shear bands (Fig. 8j), as well as intense grain size reduction within the narrow R1 shears. Comparing the microstructures, the overall grain size appears finer than in the dry anhydrite sample, even though this is not reflected by the laser particle sizer. Grain contacts are flat, as in the wet-tested mixed sample, and practically all visible grains contain intragranular plus transgranular cracks (Fig. 8j).

4. Discussion

In the following, we will compare our friction data on anhydrite, dolomite and mixed gouges with previous work, first with that done by Scuderi et al. (2013), which motivated the present work

because of its indications that gouge mixing may cause velocity-weakening behavior in wet faults in anhydrite/dolomite sequences. We go on to compare our results with a broader data set obtained on dolomite, anhydrite, as well as calcite gouges. As mentioned in the introduction, these three mineralogies share (the succession of) deformation mechanisms, and all three may be present in faults in anhydrite/dolomite formations (e.g. Alsharhan and Nairn, 1994; Collettini et al., 2009; Smith et al., 2011). Finally, we will discuss the implications of our findings for geological storage of CO₂ and for natural seismicity in the Apennines, with emphasis on the seismicity that nucleates in the interbedded anhydrite/dolomite Burano Formation.

4.1. Comparison with previous work by Scuderi et al. (2013)

Scuderi et al. (2013) performed velocity-stepping, double-direct-shear experiments in a biaxial loading frame on anhydrite, dolomite and 50:50 mixed gouges. Their samples were tested

room-dry, at room temperature and at normal stresses ranging from 10 to 150 MPa, as well as wet at 75 °C with effective normal stresses between 10 and 35 MPa. The experiments presented in the current paper differ in temperature (120 °C) and in the systematic variation employed in pore fluid type and imposed bulk shear strain rate (between 10^{-4} to 10^{-2} s $^{-1}$ here, versus 10^{-3} to 10^{-1} s $^{-1}$ by Scuderi et al.). The bulk shear strain rate is obtained by dividing velocity by the initial layer thickness (1.2 mm for the current study, and 2.8 mm for the data from Scuderi et al.). It is well established that in anhydrite an increase in temperature promotes velocity-weakening behavior, as does a decrease in strain rate (Pluymakers et al., 2014b; Pluymakers and Niemeijer, 2015). Hence, if present, any effects of mixing anhydrite and dolomite on the velocity-dependence of friction (i.e. in bringing about velocity-weakening under wet, upper crustal or CO₂ storage conditions) should be clearly visible in the current data.

Comparing the frictional strength in this study to that of Scuderi et al. (2013), obtained for wet samples at 75 °C at an effective normal stress of 20 MPa, the values for wet gouges obtained by Scuderi et al. (2013) are consistently higher than ours (by differences in μ of 0.02–0.13) for all three compositions addressed in both studies (Fig. 3c). Possible explanations may lie in differences in initial grain size (our <50 μ m versus their <150 μ m), in sample assembly, in displacement (our 2 mm versus their ~10 mm, or a shear strain of 1.7 versus 3.6) at which the strength was measured, in temperature (our 120 °C versus their 75 °C) and in normal stress (our 25 MPa versus their 20 MPa). The velocity dependence of friction for anhydrite at 80 °C is similar to that at 120 °C (Pluymakers et al., 2014b), implying the difference in temperature should not have a drastic impact on frictional strength – assuming (*a-b*) and friction can be directly correlated under the test conditions. Furthermore, Scuderi's data indicates a trend of decreasing friction coefficient with increasing normal stress, where the 5 MPa difference between the experiments could explain up to ~0.05 difference in friction coefficient. The remaining difference (i.e. up to 0.07) may be attributed to the aforementioned differences in experimental set-up and sample assembly, where the different shear strains at which the data was obtained are a likely candidate.

As recalled above, we set out to determine if, at pressure and temperature conditions relevant to CO₂ storage, the mixing of anhydrite and dolomite fault gouges could decrease (*a-b*) such that they would exhibit velocity-weakening behavior. For dry gouges

(velocity-weakening, Fig. 5a) and wet + CO₂ gouges (velocity-strengthening, Fig. 5c), we found no systematic differences concerning variations in (*a-b*) (or in trends of (*a-b*) with velocity) with composition. However, comparison between wet-tested mixed gouges (without CO₂) and the wet end-member compositions shows less marked velocity-strengthening for the mixed gouge (Fig. 5b), a decrease in (*a-b*) which is consistent with the results obtained by Scuderi et al. (2013) (see Fig. 9). Scuderi et al. explored velocities up to 300 μ m s $^{-1}$, or shear strain rates up to 10^{-1} s $^{-1}$, and found negative (*a-b*) at the high end of this strain rate range. Our data follow the same trend at shear strain rates between 10^{-4} and 10^{-2} s $^{-1}$ with a maximum at 10^{-3} s $^{-1}$ (Fig. 9). At the lowest shear strain rate investigated, 10^{-4} s $^{-1}$, wet 50:50 mixtures show lower (*a-b*) than their end-member compositions. This raises the question of whether they would exhibit velocity-weakening behavior at lower or higher velocities (similar velocity-dependent (*a-b*) are reported for serpentinite gouges, see Reinen et al., 1994). To confirm or eliminate that possibility more data at a larger range of velocities would be needed. By contrast, samples pressurized with CO₂-saturated water (not investigated by Scuderi et al.) show positive (*a-b*) over the entire strain rate range investigated, with no clear dependence of (*a-b*) on shear strain rate (Fig. 9b) and hence no increase in seismogenic potential towards higher and lower shear strain rates.

4.2. Broader comparison

In the following comparison, we only consider samples consisting of >80% pure calcite, anhydrite and dolomite and only with data from experiments performed at normal stresses up to 200 MPa and temperatures up to 200 °C. We focus on low velocity data (strain rates of 10^{-3} – 10^{-4} s $^{-1}$), which we assume to be the most representative for earthquake nucleation velocities and most comparable to the results reported here. We also restrict our attention to dry and wet samples without CO₂, as only our experiments address the effects of CO₂. All data points plus their sources are listed in Appendix Table A3 to A6.

In terms of practical use (for modeling purposes, for example), the frictional strength of all three of these minerals under the investigated P-T conditions falls close to a Byerlee friction coefficient of 0.6 (Byerlee, 1978), with friction coefficient values lying between 0.5 and 0.75, see Fig. 10 (Shimamoto and Logan, 1981;

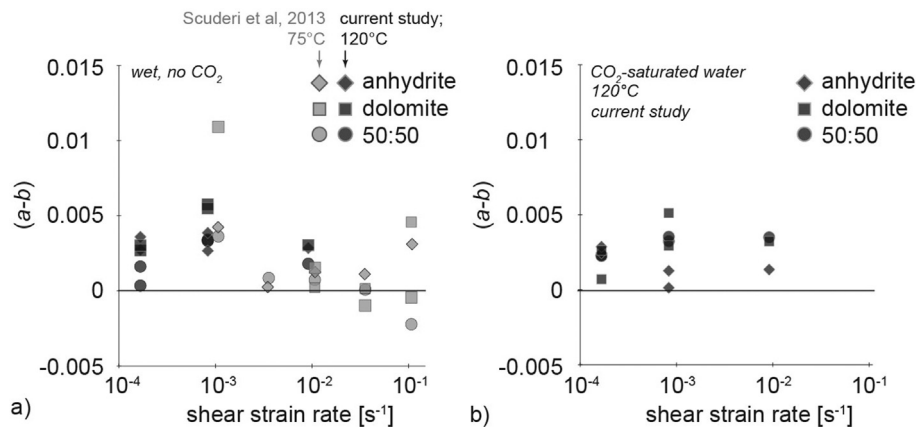


Fig. 9. a) (*a-b*) values versus bulk shear strain rate (s $^{-1}$) for wet experiments on anhydrite gouge, dolomite gouge and 50:50 mixtures. Data-points in black represent results from the current study ($T = 120$ °C, $\sigma_n = 25$ MPa). Data-points in grey are from Scuderi et al., (2013) ($T = 75$ °C, $\sigma_n = 20$ MPa). The (*a-b*) values obtained by Scuderi et al. are positive at shear strain rate of 10^{-3} s $^{-1}$, becoming negative at 10^{-1} s $^{-1}$, and our data follow the same trend between 10^{-3} and 10^{-2} s $^{-1}$ b) Data on (*a-b*) versus bulk shear strain rate (s $^{-1}$) for wet + CO₂ experiments on anhydrite, on dolomite and on 50:50 mixtures, as obtained in the current study ($T = 120$ °C, $\sigma_n = 25$ MPa) (adapted from Fig. 6c). These samples show positive (*a-b*) over the entire strain rate range investigated, with little influence of shear strain rate.

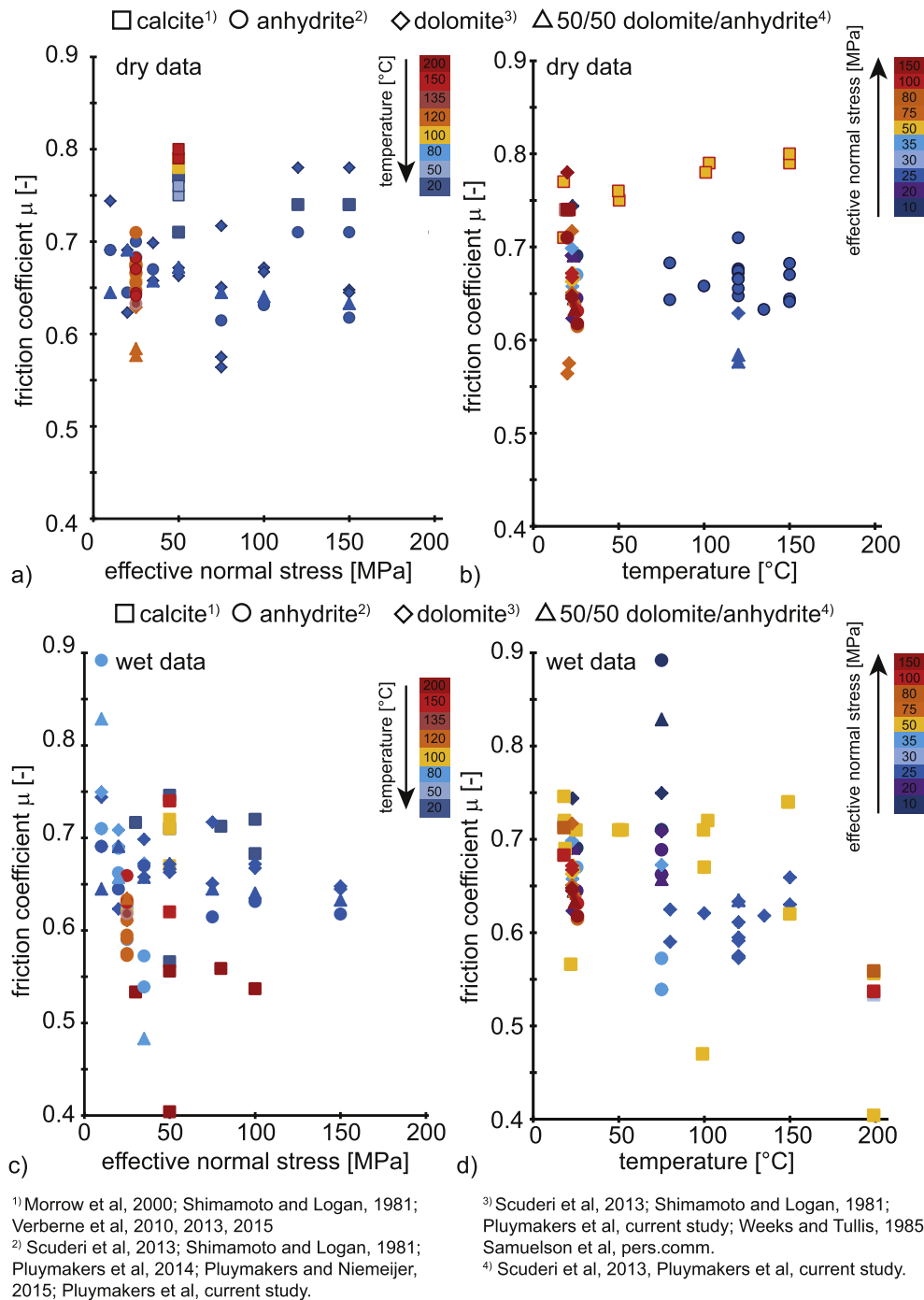


Fig. 10. Near-steady state friction coefficient values (μ) for dry and wet fault gouges (without CO_2) composed of calcite, anhydrite, dolomite and 50:50 anhydrite/dolomite mixtures. Data sources as indicated. Color coding indicates temperature or normal stress at which the experiments were performed. The majority of μ -values fall between 0.55 and 0.7, with effects of normal stress and temperature being minor. a) μ vs. normal stress for dry samples at temperatures between 20 and 200 °C. b) μ vs. temperature for dry samples at normal stresses between 10 and 150 MPa. c) μ vs. normal stress for wet samples at temperatures between 20 and 200 °C. d) μ vs. temperature for wet samples at normal stresses between 10 and 150 MPa. (For interpretation of the references to colour in this figure legend, the reader is referred to the web version of this article.)

Weeks and Tullis, 1985; Morrow et al., 2000; Verberne et al., 2010, 2013, 2015; Pluymakers et al., 2014b; Pluymakers and Niemeijer, 2015). This implies that the variability we found in our experiments, as well as the difference between our results and those of Scuderi et al., is negligible compared to the overall variability seen in these materials when tested in different settings under varying conditions. It is difficult to extract strong, common trends as a function of composition, normal stress and/or temperature (Fig. 10).

Despite the large variability in testing conditions, dolomite, anhydrite and calcite all are slightly weaker in the presence of water (Fig. 10). Possible explanations for this may lie in lubrication of grain contacts, activation of solution-transfer processes and/or an increase in grain fragmentation by promotion of subcritical microcracking. In our anhydrite we observe flat grain contacts (Fig. 8), as well as a lower porosity after testing wet compared to dry samples (Table 1). The microstructures also indicate a reduced

grain size for wet anhydrite samples, though this is not reflected by the particle size data. This could be related to clumping of the grains, i.e. increased cohesion. Even though the absolute values for porosity from the point counting method were on the high side, possibly due to drying or impregnation effects, the wet samples had consistently lower porosities than the dry ones. Based on these observations and previous work, it is likely that both subcritical microcracking and solution transfer processes were active in the wet samples.

With respect to the velocity-dependence of friction of anhydrite, dolomite and calcite gouges (Verberne et al., 2010, 2013, 2015; Scuderi et al., 2013; Pluymakers et al., 2014b; Pluymakers and Niemeijer, 2015), trends in (*a-b*) with normal stress are weak (Fig. 11). In sharp contrast, there are clear trends for (*a-b*) with increasing temperature for anhydrite and dolomite, as was found for calcite. This implies that thermally activated processes play a role in anhydrite and dolomite gouges as well, similarly to what has been suggested for calcite gouges (Niemeijer and Collettini, 2013; Verberne et al., 2013, 2015; Chen et al., 2015). Dry anhydrite gouges (tested at 25 MPa) transition from velocity-strengthening to velocity-weakening at the highest temperature of the three, being velocity-weakening around 120 °C (Fig. 11g). Dry dolomite gouge is velocity-strengthening at room temperature and velocity-weakening at 120 °C, transitioning at some intermediate temperature (Fig. 11e). In dry calcite (tested at 50 MPa), the transition from velocity-strengthening to velocity-weakening behavior occurs around ~80 °C (Fig. 11h).

Comparing the transition from velocity-strengthening to velocity-weakening between wet and dry samples, the transition temperature from velocity-strengthening to velocity-weakening is shifted upwards slightly for samples: wet calcite gouges (tested at 50 MPa) show a transition from positive to negative (*a-b*) between 100 and 150 °C (Fig. 11p) and wet dolomite (tested at 25–35 MPa) shows a transition between 120 and 150 °C (Fig. 11m). Wet anhydrite exhibits a range of (*a-b*) values at all temperatures investigated (75–150 °C), including some mildly velocity-weakening values, but tending towards stronger velocity-weakening behavior just above 150 °C (Fig. 11o) (c.f. Pluymakers et al., 2014b). Their transition temperature is correlated with the magnitude of (*a-b*): calcite has the lowest transition temperature, and exhibits the most strongly negative (*a-b*), followed by dolomite, followed by anhydrite, with the highest transition temperature and smallest (*a-b*) values. One might expect that with these ionic compounds their velocity dependence would be correlated to relative solubility (see Fig. 12) (Blount and Dickson, 1969; Plummer and Busenberg, 1982; Langmuir, 1997), or to differences in their hardness (Johnsen, 2004) or strength (Müller and Siemes, 1974; Rutter, 1974; Wenk and Shore, 1975; Barber et al., 1981; Müller et al., 1981; Schmid et al., 1987; Dell'Angelo and Olgaard, 1995; Bruhn et al., 1999; Davis et al., 2008; Delle Piane et al., 2008; Hangx et al., 2010a, 2010b, 2014). This is not the case, however, and there are no easy proxies to understand what controls the change in sign of velocity dependence. The rate-dependence of (*a-b*) (Figs. 6 and 8) indicates that time-dependent processes are active, and it is likely that the competition between time-dependent and slip-dependent processes control the transition from velocity-weakening to strengthening behavior (c.f. Niemeijer and Spiers, 2006; den Hartog and Spiers, 2014). Furthermore, characteristics of the microstructures were very similar throughout all samples, with the presence of water leading to reduced porosity, flat grain contacts and increased cohesion, especially in the anhydrite sample (Fig. 8). The most likely candidate mechanism that explains these observations is pressure solution, suggesting that the activity of pressure solution in these ionic samples promotes the occurrence of velocity strengthening behavior.

4.3. Implications

There is a striking difference between anhydrite-rich gouges and the pure dolomite gouges in the presence of water: while dolomite gouges exhibited less marked displacement weakening when wet, anhydrite gouges exhibited significant displacement weakening (Fig. 4). This suggests displacement weakening is a material property of anhydrite gouges. Note that similar tests performed in the same configuration and machine did not exhibit such strong displacement weakening (e.g. Samuelson and Spiers, 2012), indicating it is probably not related to the experimental configuration. The importance of this displacement weakening in mature (wet) anhydrite-rich faults in nature is difficult to evaluate, especially considering that the current experimental set-up allows for only small shear displacements. Additionally, the sample procedure with velocity steps is not ideal, also since the occurrence of stick-slip behavior may lead to different displacement weakening behavior (i.e. compare the dry anhydrite samples in Fig. 2a). The significance of this displacement weakening in anhydrite gouges with respect to earthquake and/or slow slip nucleation (Ikari et al., 2013; Ohnaka, 2013) deserves attention in future investigation.

4.3.1. Implications for CO₂-storage sites

For faults in an anhydrite/dolomite sequence at a depth of 3–4 km the presence of water, with or without dissolved CO₂, can be expected to lead to fault friction coefficients of 0.6–0.635 for mixed anhydrite/dolomite composition (Fig. 3), i.e. in the middle of the range of $\mu = 0.55$ to 0.7 reported for ionic gouges. The lack of strong trends in μ with temperature or normal stress implies that the values obtained in this study should be representative for natural gouges at CO₂ storage depths of 2–4 km. The presence of CO₂ may lead to slight weakening, with the worst-case scenario the values reported for wet pure anhydrite gouges pressurized with CO₂ (Pluymakers et al., 2014b), with $\mu = 0.53$.

With respect to the velocity dependence, and the associated potential for earthquake generation, the wet samples tested in the current study only exhibited velocity-strengthening behavior at 120 °C and 25 MPa normal stress. Normal stress has only a small influence on (*a-b*) (Fig. 11i, k), and the presence of CO₂ did not change the sign of velocity dependence, in line with what was reported by Pluymakers et al. (2014b). Using the velocity dependence as the most important parameter with respect to seismic potential, the increased transition temperature for wet samples implies that at a given depth (and thus temperature) in the upper crust, the seismic potential of anhydrite and carbonate formations is reduced by the presence of water. Pluymakers and Niemeijer (2015) reported for anhydrite that even damp CO₂ (i.e. CO₂ that contains some dissolved water) exhibits the velocity strengthening behavior characteristic for wet gouges. Wet or damp faults that contain anhydrite and/or dolomite gouges, with or without CO₂, at depths up to 4 km, should thus have little seismogenic potential, assuming that the investigated strain rates are representative for earthquake nucleation rates. However, in the present wet experiments CO₂ was introduced via a static pore fluid phase. Flow-through of dry CO₂ or juxtaposition of a large body of dry CO₂ against a fault may have the potential to cause desiccation (Duan and Sun, 2003; Pluymakers et al., 2014b), switching gouge behavior from wet to dry, and hence from velocity-strengthening to velocity-weakening at temperatures in the range 120–150 °C (see Fig. 10). Assessing the implications of the present results for CO₂ storage systems therefore reduces to evaluating whether faults in such systems are likely to be dry or wet under in-situ storage conditions.

It is generally expected, especially in the case of depleted oil and gas reservoirs, that, even post-injection, much of the CO₂ will be present as a free supercritical phase, structurally or

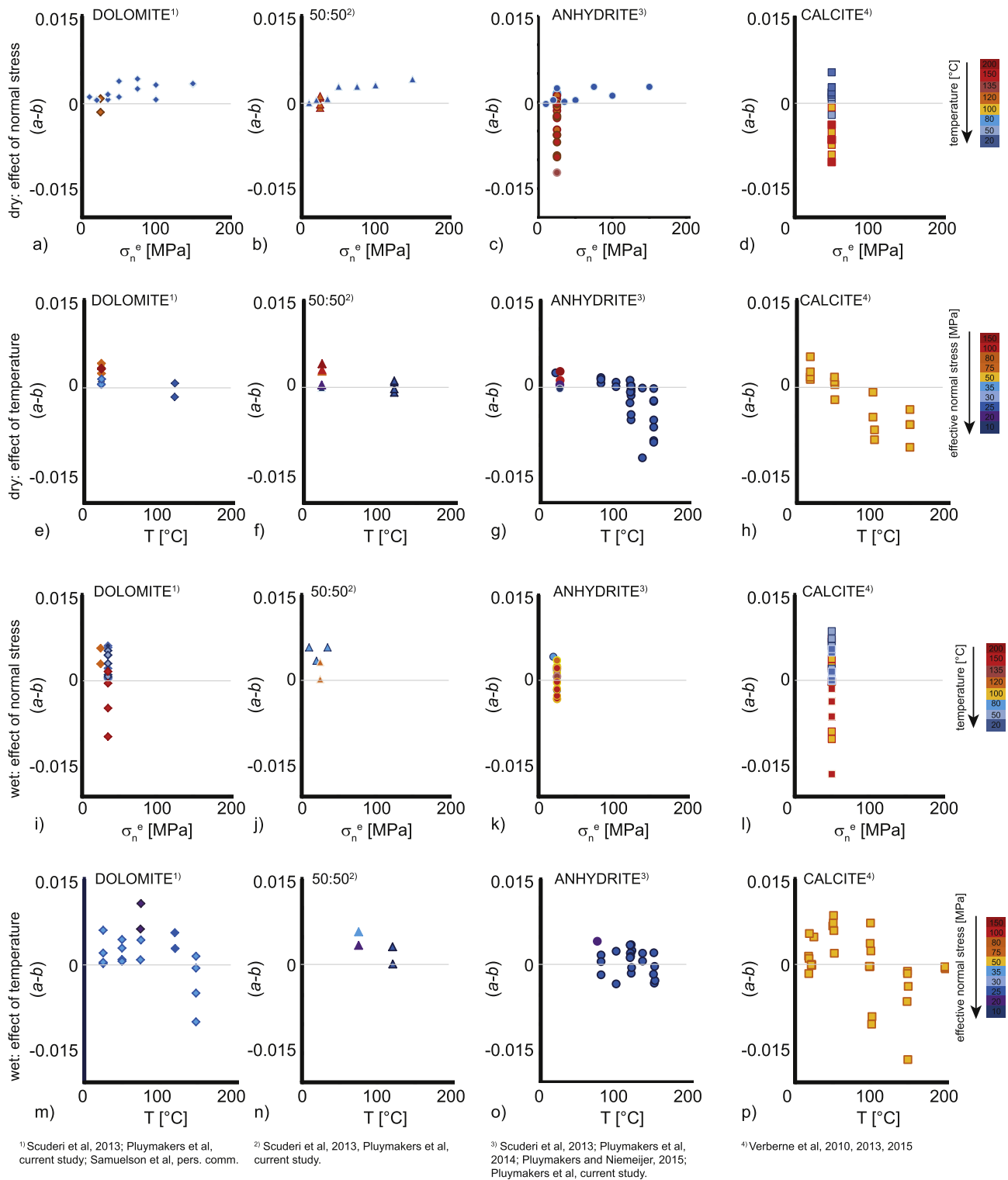


Fig. 11. Velocity-dependence of friction for dry and wet fault gouges (without CO₂) composed of dolomite, 50:50 anhydrite/dolomite, anhydrite and calcite. Color coding indicates temperature or normal stress at which the experiments are performed. Gouge type is indicated at the top of each graph, data sources at the bottom. a–d) Data on (a–b) vs. normal stress for dry samples at temperatures between 20 and 200 °C. e–h) Data on (a–b) vs. temperature for dry samples at normal stresses between 10 and 150 MPa. i–l) Data on (a–b) vs. normal stress for wet samples at temperatures between 20 and 200 °C. m–p) Data on (a–b) vs. temperature for wet samples at normal stresses between 10 and 150 MPa. (For interpretation of the references to colour in this figure legend, the reader is referred to the web version of this article.)

stratigraphically trapped by the caprock (Gaus, 2010). This is confirmed by natural analogs such as the Fizzy field (off-shore United Kingdom) (Wilkinson et al., 2009). Detailed mineralogical analyses suggests that most of the CO₂ present existed as a free

supercritical phase since charging more than 50 Ma ago. In contrast to such a natural analog, at a given CO₂ storage-site, the injected CO₂ will be dry, to avoid corrosion of the transport pipelines and/or tanker trucks. Over time, some of this initially dry CO₂ will dissolve

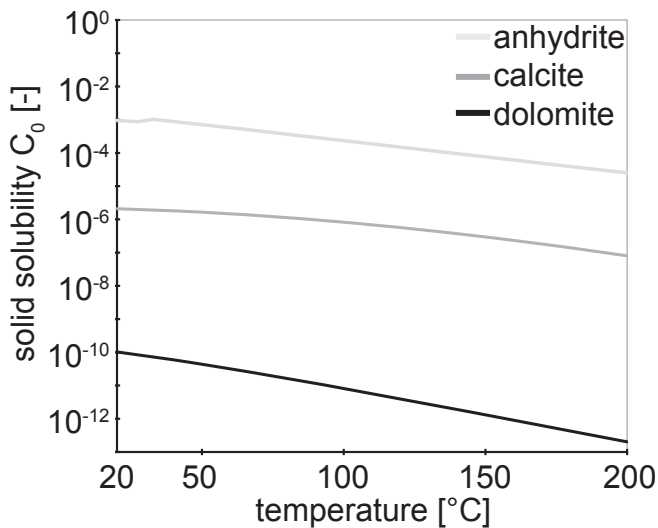


Fig. 12. Solubility of anhydrite (Blount and Dickson, 1969), calcite (Plummer and Busenberg, 1982) and dolomite (Langmuir, 1997, p.206) as a function of temperature in water, at atmospheric pressure or, above 100 °C, at the vapor pressure of water above the solution phase. Solubility values are given in units of m^3/m^3 , calculated by multiplying the solubility (mol m^{-3}) by the molar volume ($\text{m}^3 \text{mol}^{-1}$).

in the formation water and/or react with the minerals in the reservoir, and some water will dissolve in the injected CO_2 (e.g. Spycher et al., 2003). The extent to which mutual dissolution occurs depends on local conditions, including the injection rate, porosity, permeability, the dissolution kinetics (hence pressure and temperature), pore fluid composition and finally the reservoir composition (i.e. reactive mineral content) (Rochelle et al., 2004; Gaus, 2010). On the basis of geochemical modeling, it has been inferred that long-term CO_2 -injection in an initially wet subsurface reservoir will lead to a chimney of dry (supercritical) CO_2 , surrounded by progressively wetter CO_2 – even for injection into saline aquifers (Johnson et al., 2004; Rochelle et al., 2004). The presence of (some) dry CO_2 in a storage scenario in a depleted gas reservoir thus seems possible, especially within a few meters of the injection well (c.f. Schaef et al., 2012; Miller et al., 2013). In the case of reservoirs or aquifers topped by anhydrite/dolomite caprocks, this emphasizes the need to ascertain that the injection-point is not too close to detectable faults, especially as near-fault injection may significantly perturb the local stress, strain and temperature field. Precautionary measures could include modeling the expected migration path and thermomechanical impact of the CO_2 -plume, including an assessment of the volume that may be dry.

Long-term effects of the presence of CO_2 could include reaction of anhydrite with CO_2 and water to form calcite (c.f. Hangx et al., 2010a; Orlic et al., 2011; Pluymakers and Spiers, 2015). Most work to date shows little to no calcite formation (Czernichowski-Lauriol et al., 1996; Rochelle et al., 2004; Kuhn et al., 2009; Hangx et al., 2010a; Pluymakers et al., 2014a) in anhydrite-rich rocks without an alkaline source, though more work is needed to establish whether or not this reaction will take place for realistic reservoir compositions. If calcite is formed in sufficient amounts in an anhydrite/dolomite sequence, it may also lead to velocity-weakening slip (Verberne et al., 2010, 2013) at temperatures between 80 and 120 °C, i.e. depths of 2.5–4 km (Fig. 11).

4.3.2. Implications for seismicity in the Italian Apennines

The present results on the frictional properties of anhydrite and dolomite are also applicable to the seismicity nucleating at depths of 5–10 km in the Burano Formation of Italian Apennines (e.g.

Mirabella et al., 2008; Collettini et al., 2009; Speranza and Minelli, 2014), since the active normal faults in the region are expected to contain anhydrite and dolomite gouges (Collettini et al., 2008, 2009; De Paola et al., 2009). Temperatures at seismogenic depths in the region are expected to lie between 100 and 300 °C, and, due to the high pressure CO_2 -rich fluids present at depth in the region (e.g. Trippetta et al., 2013), effective normal stresses on the normal faults could be as low as 20 MPa. Our results, combined with previous work (Fig. 11), indicate that dry fault gouges, derived from anhydrite and dolomite, will show velocity-weakening behavior across this full range of temperatures and depth (i.e. 5–10 km). Wet anhydrite and dolomite gouges will only exhibit velocity-weakening behavior at temperatures above 150 °C (i.e. at depths >6 km). At depths <6 km, wet anhydrite/dolomite gouges are expected to deform aseptically (creep) (Fig. 11). Earthquake nucleation in the shallower part of the Apennines thus needs additional explanations, such as an effect of normal stress (as suggested by the few datapoints in Fig. 11i, k). Desiccation by the high CO_2 -fluxes present in the region (e.g. Chiodini et al., 2004) seems unlikely, since these fluxes are related to metasomatism by crustal fluids of mantle rocks overlying the Adriatic subduction zone (Chiodini et al., 2004; Collettini et al., 2009). Alternative explanations for the shallow (and perhaps some of the deeper) seismic behavior seen in the Apennines include a role played by a) marked slip weakening effects following reactivation (not explored) (c.f. Ikari et al., 2013; Ohnaka, 2013), similar to that seen in our experiments and in previous experiments on anhydrite gouges (Pluymakers et al., 2014b), or b) calcite present in the system, which showed velocity-weakening behavior from 100 °C (Fig. 11). As pointed out by Verberne et al. (2013), this corresponds to the top of the seismogenic zone in the Apennines. For calcite, ($a-b$) values are more strongly negative than for dolomite, and dolomite exhibits more strongly negative ($a-b$) than anhydrite (Fig. 11). Correlating the magnitude of ($a-b$) with earthquake magnitude (Dieterich, 1972; Scholz and Engeler, 1976; Marone, 1998; Scholz, 2002), this implies that for earthquake nucleation in the Apennines the role of dolomite (and/or calcite) may be more important than that of anhydrite.

5. Conclusions

Direct shear experiments have been conducted on simulated gouges composed of anhydrite, dolomite and 50:50 wt% mixtures of these two, under vacuum-dry and wet conditions, as well as on wet gouges pressurized with CO_2 . These materials can be expected to control the frictional behavior of fault zones cutting anhydrite/dolomite caprocks overlying CO_2 -storage reservoirs, as well as natural seismicity nucleating in anhydrite/dolomite-rich formations found in tectonically active regions, such as the Italian Apennines. The experiments were carried out at 120 °C and an effective normal stress σ_n^e of 25 MPa, and sliding velocities between 0.21 and 11 $\mu\text{m s}^{-1}$, attaining displacements up to ~6 mm. In addition to presenting new data, we compared our results on the frictional strength and velocity-dependence of friction with previous data for anhydrite, dolomite and anhydrite/dolomite gouges, as well as data for calcite gouges. We found the following:

- 1) After macroscopic yield, all samples showed a near steady-state frictional strength μ in the range 0.55–0.71. All gouges tended to be slightly weaker in the presence of water, and weaker still in the presence of CO_2 -saturated water, though with the frictional strength still falling in the above range. The 50:50 anhydrite/dolomite gouge exhibited a frictional strength similar to dolomite ($\mu \sim 0.625$ when dry, $\mu \sim 0.61$ when wet). Anhydrite was found to be slightly stronger than both anhydrite/dolomite and

- dolomite gouges when dry ($\mu=0.69$), and slightly weaker than both when wet (~ 0.57).
- 2) All dry gouges exhibited velocity-weakening behavior, whereas all gouges tested wet, with or without CO_2 exhibited velocity-strengthening behavior at the conditions studied. The wet gouges showed an effect of mixing, displaying a slight decrease in the velocity dependence of friction, i.e. in ($a-b$) values, for mixed gouges compared with anhydrite and dolomite end-member compositions, though ($a-b$) remains positive across the range of velocities studied.
 - 3) Despite differences in conditions and sample set-up, our results indicate that ($a-b$) for wet anhydrite, dolomite and mixed fault gouges, without CO_2 , exhibits similar trends with composition and shear strain rate as seen in the data presented by Scuderi et al. (2013).
 - 4) Comparison with literature data indicates that temperature is a stronger control than normal stress on the transition from velocity-strengthening to velocity-weakening behavior in anhydrite, dolomite and also in calcite gouges. When dry, all three minerals show a transition from velocity-strengthening to velocity-weakening behavior in the range $80\text{--}120^\circ\text{C}$.
 - 5) In a CO_2 -storage scenario at 2–4 km depth, expected temperatures will be $80\text{--}120^\circ\text{C}$, i.e. in a range where only dry anhydrite and/or dolomite gouges exhibit velocity-weakening behavior at laboratory sliding rates. Some dry CO_2 is expected within meters distance of the injection well. Aside from injection-related stress and temperature changes which can potentially promote fault reactivation, the possibility of fault zone desiccation by dry CO_2 accordingly presents an additional reason not to place an injection well close to (detectable) faults. For persistently wet fault zones, little seismogenic potential for dolomite, anhydrite and mixed composition gouges is expected, whether in contact with CO_2 or not.
 - 6) The review of literature data furthermore indicated that the anhydrite/dolomite fault zones in the Italian Apennines fault zones will most likely contain water. Hypocentral depths are 5–10 km, and for earthquakes deeper than ~ 6 km, where temperatures are expected above 150°C , the velocity-weakening behavior of wet dolomite and anhydrite that is previously reported to occur at these temperatures is consistent with earthquake nucleation. For the shallower seismicity, nucleation mechanisms may include the stronger potential for velocity-weakening of anhydrite/dolomite mixtures. Another possibility is a role played by (wet) calcite (above and below 6 km), which has been reported previously to exhibit velocity-weakening behavior from 100°C .

Acknowledgments

Data used in this paper were acquired during laboratory experiments performed at the High Pressure and Temperature Laboratory at Utrecht University, the Netherlands. The research was performed within WorkPackage 3.3 (Caprock and Fault Integrity) of the Dutch national CCS research program CATO-2. ARN is supported by ERC starting grant SEISMIC (nr. 335915) and by the Dutch Foundation for Scientific Research (NWO) through a VIDI grant (nr. 854.12.011). The funding sources had no influence in study design and subsequent data collection and writing up. We thank Jan Penninga (Nederlandse Aardolie Maatschappij B.V.) and Suzanne Hangx (Shell Global Solutions) for supplying the sample material. We also thank Eimert de Graaff, Gert Kastelein, Peter van Krieken and Mariska Schimmel for technical assistance. We thank the Editor, Toru Takeshita, and the Reviewers, Matt Ikari and Marco Scuderi, for their constructive comments.

Appendix A. Supplementary data

Supplementary data related to this article can be found at <http://dx.doi.org/10.1016/j.jsg.2015.11.008>.

References

- Alsharhan, A.S., Nairn, A.E.M., 1994. The late Permian carbonates (Khuff Formation) in the western Arabian Gulf: Its hydrocarbon parameters and paleogeographical aspects. *Carbonates Evaporites* 9, 132–142. <http://dx.doi.org/10.1007/BF03175226>.
- Bai, G., Xu, Y., 2014. Giant fields retain dominance in reserves growth. *Oil Gas J.* 112.
- Barber, D.J., Heard, H.C., Wenk, H.R., 1981. Deformation of dolomite single crystals from $20\text{--}800^\circ\text{C}$. *Phys. Chem. Min.* 7, 271–286. <http://dx.doi.org/10.1007/BF00311980>.
- Barbot, S., Lapusta, N., Avouac, J.-P., 2012. Under the hood of the earthquake machine: toward predictive modeling of the seismic cycle. *Science* 336, 707–710. <http://dx.doi.org/10.1126/science.1218796>.
- Bennion, B., Bachu, S., 2013. Drainage and imbibition relative permeability relationships for supercritical CO_2 /Brine and H_2S /Brine systems in intergranular Sandstone, carbonate, shale, and anhydrite rocks. *SPE Reserv. Eval. Eng.* 11, 487–496. <http://dx.doi.org/10.2118/99326-PA>.
- Blount, C.W., Dickson, F.W., 1969. The solubility of anhydrite (CaSO_4) in $\text{NaCl}\text{--}\text{H}_2\text{O}$ from 100 to 450°C and 1 to 1000 bars. *Geochim. Cosmochim. Acta* 33, 227–245. [http://dx.doi.org/10.1016/0016-7037\(69\)90140-9](http://dx.doi.org/10.1016/0016-7037(69)90140-9).
- Bruhn, D.F., Olgaard, D.L., Dell'Angelo, L.N., 1999. Evidence for enhanced deformation in two-phase rocks: experiments on the rheology of calcite-anhydrite aggregates. *J. Geophys. Res.* 104, 707. <http://dx.doi.org/10.1029/98JB02847>.
- Byerlee, J., 1978. Friction of rocks. *Pure Appl. Geophys. PAGEOPH* 116, 615–626. <http://dx.doi.org/10.1007/BF00876528>.
- Chen, J., Verberne, B.A., Spiers, C.J., 2015. Interseismic re-strengthening and stabilization of carbonate faults by “non-Dieterich” healing under hydrothermal conditions. *Earth Planet. Sci. Lett.* 423, 1–12. <http://dx.doi.org/10.1016/j.epsl.2015.03.044>.
- Chiodini, G., Cardellini, C., Amato, A., Boschi, E., Caliro, S., Frondini, F., Ventura, G., 2004. Carbon dioxide Earth degassing and seismogenesis in central and southern Italy. *Geophys. Res. Lett.* 31, L07615. <http://dx.doi.org/10.1029/2004gl019480>.
- Chiodini, G., Frondini, F., Kerrick, D.M., Rogie, J., Parello, F., Peruzzi, L., Zanzari, A.R., 1999. Quantification of deep CO_2 fluxes from Central Italy. Examples of carbon balance for regional aquifers and of soil diffuse degassing. *Chem. Geol.* 159, 205–222. [http://dx.doi.org/10.1016/S0009-2541\(99\)00030-3](http://dx.doi.org/10.1016/S0009-2541(99)00030-3).
- Collettini, C., Cardellini, C., Chiodini, G., De Paola, N., Holdsworth, R.E., Smith, S.A.F., 2008. Fault weakening due to CO_2 degassing in the Northern Apennines: short- and long-term processes. *Geol. Soc. Lond. Spec. Publ.* 299, 175–194. <http://dx.doi.org/10.1144/sp299.11>.
- Collettini, C., De Paola, N., Faulkner, D.R., 2009. Insights on the geometry and mechanics of the Umbria-Marche earthquakes (Central Italy) from the integration of field and laboratory data. *Tectonophysics* 476, 99–109. <http://dx.doi.org/10.1016/j.tecto.2008.08.013>.
- Czernichowski-Lauriol, I., San Juan, B., Rochelle, C., Bateman, K., Pearce, J., Blackwell, P., 1996. The Underground Disposal of Carbon Dioxide Final Report of Joule II Project Number CT92-0031, Inorganic Geochemistry.
- Davis, N.E., Kronenberg, A.K., Newman, J., 2008. Plasticity and diffusion creep of dolomite. *Tectonophysics* 456, 127–146. <http://dx.doi.org/10.1016/j.tecto.2008.02.002>.
- De Paola, N., Collettini, C., Faulkner, D.R., Trippetta, F., 2008. Fault zone architecture and deformation processes within evaporitic rocks in the upper crust. *Tectonics* 27, TC4017. <http://dx.doi.org/10.1029/2007tc002230>.
- De Paola, N., Faulkner, D.R., Collettini, C., 2009. Brittle versus ductile deformation as the main control on the transport properties of low-porosity anhydrite rocks. *J. Geophys. Res.* 114, B06211. <http://dx.doi.org/10.1029/2008jb005967>.
- Dell'Angelo, L.N., Olgaard, D.L., 1995. Experimental deformation of fine-grained anhydrite: evidence for dislocation and diffusion creep. *J. Geophys. Res.* 100, 15425–15440. <http://dx.doi.org/10.1029/95jb00956>.
- Delle Piane, C., Burlini, L., Kunze, K., Brack, P., Burg, J.P., 2008. Rheology of dolomite: large strain torsion experiments and natural examples. *J. Struct. Geol.* 30, 767–776. <http://dx.doi.org/10.1016/j.jsg.2008.02.018>.
- den Hartog, S.A.M., Spiers, C.J., 2014. A microphysical model for fault gouge friction applied to subduction megathrusts. *J. Geophys. Res. Solid Earth* 119. <http://dx.doi.org/10.1002/2013jb010580>.
- Dieterich, J.H., 1979. Modeling of rock friction: 1. Experimental results and constitutive equations. *J. Geophys. Res.* 84, 2161–2168. <http://dx.doi.org/10.1029/JB084iB05p02161>.
- Dieterich, J.H., 1978. Time-dependent friction and the mechanics of stick-slip. *Pure Appl. Geophys.* 116, 790–806. <http://dx.doi.org/10.1007/BF00876539>.
- Dieterich, J.H., 1972. Time-dependent friction as a possible mechanism for after-shocks. *J. Geophys. Res.* 77, 3771–3781. <http://dx.doi.org/10.1029/JB077i020p03771>.
- Duan, Z., Sun, R., 2003. An improved model calculating CO_2 solubility in pure water and aqueous NaCl solutions from 273 to 533 K and from 0 to 2000 bar. *Chem. Geol.* 193, 257–271. [http://dx.doi.org/10.1016/S0009-2541\(02\)00263-2](http://dx.doi.org/10.1016/S0009-2541(02)00263-2).
- Gaus, I., 2010. Role and impact of CO_2 –rock interactions during CO_2 storage in

- sedimentary rocks. *Int. J. Greenh. Gas. Control* 4, 73–89. <http://dx.doi.org/10.1016/j.ijggc.2009.09.015>.
- Geluk, M.C., 2007. Permian, Geology of the Netherlands. Royal Netherlands. Academy of Arts and Sciences, Amsterdam, Netherlands.
- Geluk, M.C., 2000. Late Permian (Zechstein) carbonate-facies maps the Netherlands. *Geol. Netherl. J. Geosci.* 79, 17–27.
- Hangx, S.J.T., Pluymakers, A., ten Hove, A., Spiers, C.J., 2014. Effects of lateral variations in rock composition and texture on anhydrite caprock integrity of CO₂ storage systems. *Int. J. Rock Mech. Min. Sci.* 69, 80–92. <http://dx.doi.org/10.1016/j.ijrmms.2014.03.001>.
- Hangx, S.J.T., Spiers, C.J., Peach, C.J., 2010a. Mechanical behavior of anhydrite caprock and implications for CO₂ sealing capacity. *J. Geophys. Res.* 115, B07402. <http://dx.doi.org/10.1029/2009jb006954>.
- Hangx, S.J.T., Spiers, C.J., Peach, C.J., 2010b. The effect of deformation on permeability development in anhydrite and implications for caprock integrity during geological storage of CO₂. *Geofluids* 10, 369–387. <http://dx.doi.org/10.1111/j.1468-8123.2010.00299.x>.
- Ikari, M.J., Marone, C., Saffer, D.M., Kopf, A.J., 2013. Slip weakening as a mechanism for slow earthquakes. *Nat. Geosci.* 6, 468–472. <http://dx.doi.org/10.1038/ngeo1818>.
- Improta, L., De Gori, P., Chiarabba, C., 2014. New insights into crustal structure, cenozoic magmatism, CO₂ degassing and seismogenesis in the southern apennines and irpinia region from local earthquake tomography. *J. Geophys. Res. Solid Earth* 8283–8311. <http://dx.doi.org/10.1002/2013JB010890>.
- Johnsen, O., 2004. *Minerals of the World*. Princeton University Press, Princeton.
- Johnson, J.W., Nitao, J.J., Knauss, K.G., 2004. Reactive transport modelling of CO₂ storage in saline aquifers to elucidate fundamental processes, trapping mechanisms and sequestration partitioning. *Geol. Soc. Lond. Spec. Publ.* 233, 107–128. <http://dx.doi.org/10.1144/GSL.SP.2004.233.01.08>.
- Kuhn, M., Vosbeck, K., Meyn, V., Back, M., Clauser, C., Stanjek, H., Peiffer, S., 2009. Mineral trapping of CO₂ in operated hydrothermal reservoirs. In: Grobe, M., Pashin, J.C., Dodge, R.L. (Eds.), *AAPG Studies in Geology* 59. American Association of Petroleum Geologists, pp. 545–553. Tulsa, OK.
- Langmuir, D., 1997. *Aqueous Environmental Geochemistry*. Prentice Hall, Upon Saddle River, New Jersey.
- Logan, J.M., Friedman, M., Higgs, N., Dengo, C., Shimamoto, T., 1979. Experimental studies of simulated gouge and their application to studies of natural fault zones. In: Survey, U.S.G. (Ed.), *Proceedings of Conference VIII, Analysis of Actual Fault Zones in Bedrock*, pp. 305–343.
- Marone, C., 1998. The effect of loading rate on static friction and the rate of fault healing during the earthquake cycle. *Nature* 391, 69–72. <http://dx.doi.org/10.1038/34157>.
- Miller, Q.R.S., Thompson, C.J., Loring, J.S., Windisch, C.F., Bowden, M.E., Hoyt, D.W., Hu, J.Z., Arey, B.W., Rosso, K.M., Schaeff, H.T., 2013. Insights into silicate carbonation processes in water-bearing supercritical CO₂ fluids. *Int. J. Greenh. Gas. Control* 15, 104–118. <http://dx.doi.org/10.1016/j.ijggc.2013.02.005>.
- Miocic, J.M., Gillilan, S.M.V., McDermott, C., Haszeldine, R.S., 2013. mechanisms for CO₂ leakage prevention: A global dataset of natural analogues. *Energy Procedia* 40, 320–328. <http://dx.doi.org/10.1016/j.egypro.2013.08.037>.
- Mirabella, F., Barchi, M.R., Lupatelli, A., 2008. Seismic reflection data in the umbria marche region: limits and capabilities to unravel the subsurface structure in a seismically active area. *Ann. Geophys.* 51. <http://dx.doi.org/10.4401/ag-3032>.
- Mohs, F., 1820. *The Characters of the Classes, Orders, Genera, and Species: or, the Characteristic of the Natural History System of Mineralogy. Intended to Enable Student of Discriminate Minerals on Principles Similar to Those of Botany and Zoology*. Caledonian Mercury Press, Edinburgh.
- Morrow, C.A., Moore, D.E., Lockner, D.A., 2000. The effect of mineral bond strength and adsorbed water on fault gouge frictional strength. *Geophys. Res. Lett.* 27, 815–818. <http://dx.doi.org/10.1029/1999GL008401>.
- Müller, P., Siemes, H., 1974. Festigkeit, verformbarkeit und gefügeregelung von anhydrit — experimentelle stauchverformung unter manteldrücken bis 5 kbar bei temperaturen bis 300°C. *Tectonophysics* 23, 105–127. [http://dx.doi.org/10.1016/0040-1951\(74\)90114-0](http://dx.doi.org/10.1016/0040-1951(74)90114-0).
- Müller, W.H., Schmid, S.M., Briegel, U., 1981. Deformation experiments on anhydrite rocks of different grain sizes: rheology and microfabric. *Tectonophysics* 78, 527–543. [http://dx.doi.org/10.1016/0040-1951\(81\)90027-5](http://dx.doi.org/10.1016/0040-1951(81)90027-5).
- Niemeijer, A.R., Collettini, C., 2013. Frictional properties of a low-angle normal fault under in situ conditions: thermally-activated velocity weakening. *Pure Appl. Geophys.* <http://dx.doi.org/10.1007/s00024-013-0759-6>.
- Niemeijer, A.R., Spiers, C.J., 2006. Velocity dependence of strength and healing behaviour in simulated phyllosilicate-bearing fault gouge. *Tectonophysics* 427, 231–253. <http://dx.doi.org/10.1016/j.tecto.2006.03.048>.
- Niemeijer, A.R., Vissers, R.L.M., 2014. Earthquake rupture propagation inferred from the spatial distribution of fault rock frictional properties. *Earth Planet. Sci. Lett.* 396, 154–164. <http://dx.doi.org/10.1016/j.epsl.2014.04.010>.
- Noda, H., Lapusta, N., 2013. Stable creeping fault segments can become destructive as a result of dynamic weakening. *Nature* 493, 518–521. <http://dx.doi.org/10.1038/nature11703>.
- Ohnaka, M., 2013. *The Physics of Rock Failure and Earthquakes | Solid Earth Geophysics*. Cambridge University Press, Cambridge, UK. Cambridge University Press.
- Orlic, B., Ter Heege, J., Wassing, B.B.T., 2011. Assessing the short-term and long-term integrity of top seals in feasibility studies of geological CO₂ storage. *Rock Mech. Geomech. Symp.* <http://dx.doi.org/ARMA-11-375>.
- Plummer, L.N., Busenberg, E., 1982. The solubilities of calcite, aragonite and vaterite in CO₂-H₂O solutions between 0 and 90°C, and an evaluation of the aqueous model for the system CaCO₃-CO₂-H₂O. *Geochim. Cosmochim. Acta* 46, 1011–1040. [http://dx.doi.org/10.1016/0016-7037\(82\)90056-4](http://dx.doi.org/10.1016/0016-7037(82)90056-4).
- Pluymakers, A., Peach, C.J., Spiers, C.J., 2014a. Diagenetic compaction experiments on simulated anhydrite fault gouge under static conditions. *J. Geophys. Res.* B5, 4123–4148. <http://dx.doi.org/10.1002/2014JB011073>.
- Pluymakers, A., Samuelson, J.E., Niemeijer, A.R., Spiers, C.J., 2014b. Effects of temperature and CO₂ on the frictional behavior of simulated anhydrite fault rock. *J. Geophys. Res. Solid Earth* 119, 8728–8747. <http://dx.doi.org/10.1002/2014JB011575>.
- Pluymakers, A., Spiers, C.J., 2015. Compaction creep of simulated anhydrite fault gouge by pressure solution: theory vs. experiments and implications for fault sealing. *Geol. Soc. Lond. Spec. Publ.* 409, 107–124. <http://dx.doi.org/10.1144/SP409.6>.
- Pluymakers, A.M.H., Niemeijer, A.R., 2015. Healing and sliding stability of simulated anhydrite fault gouge: effects of water, temperature and CO₂. *Tectonophysics* 656, 111–130. <http://dx.doi.org/10.1016/j.tecto.2015.06.012>.
- Reinen, L.A., Weeks, J.D., 1993. Determination of rock friction constitutive parameters using an iterative least squares inversion method. *J. Geophys. Res.* 98, 15937. <http://dx.doi.org/10.1029/93JB00780>.
- Reinen, L.A., Weeks, J.D., Tullis, T.E., 1994. The frictional behavior of lizardite and antigorite serpentinites: experiments, constitutive models, and implications for natural faults. *Pure Appl. Geophys.* 143, 317–358. <http://dx.doi.org/10.1007/BF00874334>.
- Rochelle, C.A., Czernichowski-Lauriol, I., Milodowski, A.E., 2004. The impact of chemical reactions on CO₂ storage in geological formations: a brief review. *Geol. Soc. Lond. Spec. Publ.* 233, 87–106. <http://dx.doi.org/10.1144/GSL.SP.2004.233.01.07>.
- Ruina, A., 1983. Slip instability and state variable friction laws. *J. Geophys. Res.* 88, 10359–10370.
- Rutter, E.H., 1974. The influence of temperature, strain rate and interstitial water in the experimental deformation of calcite rocks. *Tectonophysics* 22, 311–334. [http://dx.doi.org/10.1016/0040-1951\(74\)90089-4](http://dx.doi.org/10.1016/0040-1951(74)90089-4).
- Saffer, D.M., Marone, C., 2003. Comparison of smectite- and illite-rich gouge frictional properties: application to the updip limit of the seismogenic zone along subduction megathrusts. *Earth Planet. Sci. Lett.* 215, 219–235. [http://dx.doi.org/10.1016/S0012-821X\(03\)00424-2](http://dx.doi.org/10.1016/S0012-821X(03)00424-2).
- Samuelson, J., Spiers, C.J., 2012. Fault friction and slip stability not affected by CO₂ storage: evidence from short-term laboratory experiments on North Sea reservoir sandstones and caprocks. *Int. J. Greenh. Gas. Control* 11, S78–S90. <http://dx.doi.org/10.1016/j.ijggc.2012.09.018>.
- Schaeff, H.T., Ilton, E.S., Qafoku, O., Martin, P.F., Felmy, A.R., Rosso, K.M., 2012. In situ XRD study of Ca²⁺-saturated montmorillonite (STX-1) exposed to anhydrous and wet supercritical carbon dioxide. *Int. J. Greenh. Gas. Control* 6, 220–229. <http://dx.doi.org/10.1016/j.ijggc.2011.11.001>.
- Schmid, S.M., Panozzo, R., Bauer, S., 1987. Simple shear experiments on calcite rocks: rheology and microfabric. *J. Struct. Geol.* 9, 747–778. [http://dx.doi.org/10.1016/0191-8141\(87\)90157-X](http://dx.doi.org/10.1016/0191-8141(87)90157-X).
- Scholz, C.H., 2002. *The Mechanics of Earthquakes and Faulting*. Cambridge University Press, Cambridge.
- Scholz, C.H., Engelder, J.T., 1976. The role of asperity indentation and ploughing in rock friction - I. Asperity creep and stick-slip. *Int. J. Rock Mech. Min. Sci.* 13, 149–154. [http://dx.doi.org/10.1016/0148-9062\(76\)90819-6](http://dx.doi.org/10.1016/0148-9062(76)90819-6).
- Scuderi, M.M., Niemeijer, A.R., Collettini, C., Marone, C., 2013. Frictional properties and slip stability of active faults within carbonate–evaporite sequences: The role of dolomite and anhydrite. *Earth Planet. Sci. Lett.* 369–370, 220–232. <http://dx.doi.org/10.1016/j.epsl.2013.03.024>.
- Shimamoto, T., Logan, J.M., 1981. Effects of simulated fault gouge on the sliding behavior of Tennessee Sandstone: Nonclay gouges. *J. Geophys. Res.* 86, 2902. <http://dx.doi.org/10.1029/JB086iB04p02902>.
- Smith, S.A., Sorensen, J.A., Steadman, E.N., Harju, J.A., Ryan, D., 2011. Zama acid gas EOR, CO₂ sequestration, and monitoring project. *Energy Procedia* 4, 3957–3964. <http://dx.doi.org/10.1016/j.egypro.2011.02.335>.
- Sone, H., Shimamoto, T., 2009. Frictional resistance of faults during accelerating and decelerating earthquake slip. *Nat. Geosci.* 2, 705–708. <http://dx.doi.org/10.1038/ngeo637>.
- Speranza, F., Minelli, L., 2014. Ultra-thick Triassic dolomites control rupture behaviour of the central Apennine seismicity: evidence from magnetic modelling of the L'Aquila fault zone. *J. Geophys. Res. Solid Earth* 119, 6756–6770. <http://dx.doi.org/10.1002/2014JB011199> n/a–n/a.
- Spycher, N., Pruess, K., Ennis-King, J., 2003. CO₂-H₂O mixtures in the geological sequestration of CO₂. I. assessment and calculation of mutual solubilities from 12 to 100°C and up to 600 bar. *Geochim. Cosmochim. Acta* 67, 3015–3031. [http://dx.doi.org/10.1016/S0016-7037\(03\)00273-4](http://dx.doi.org/10.1016/S0016-7037(03)00273-4).
- Tabor, D., 1970. The hardness of solids. *Rev. Phys. Technol.* 1, 145–179. <http://dx.doi.org/10.1088/0034-6683/1/3/101>.
- Tabor, D., 1956. The physical meaning of indentation and scratch hardness. *Br. J. Appl. Phys.* 7, 159–166. <http://dx.doi.org/10.1088/0508-3443/7/5/301>.
- Taylor, E.W., 1949. Correlation of the Mohs's scale of hardness with the Vickers's hardness numbers. *Mineral. Mag.* 28, 718–721.
- Trippetta, F., Collettini, C., Barchi, M.R., Lupatelli, A., Mirabella, F., 2013. A multidisciplinary study of a natural example of a CO₂ geological reservoir in central Italy. *Int. J. Greenh. Gas. Control* 12, 72–83. <http://dx.doi.org/10.1016/j.ijggc.2012.11.010>.
- Verberne, B.A., He, C., Spiers, C.J., 2010. Frictional properties of sedimentary rocks

- and natural fault gouge from the Longmenshan fault zone, Sichuan, China. *Bull. Seismol. Soc. Am.* 100, 2767–2790. <http://dx.doi.org/10.1785/0120090287>.
- Verberne, B.A., Niemeijer, A.R., De Bresser, J.H.P., Spiers, C.J., 2015. Mechanical behaviour and microstructure of simulated calcite fault gouge sheared at 20–600 °C: Implications for natural faults in limestones. *J. Geophys. Res. Solid Earth*. <http://dx.doi.org/10.1002/2015JB012292> (in press).
- Verberne, B.A., Spiers, C.J., Niemeijer, A., De Bresser, J.H.P., De Winter, D.A.M., Plümper, O., 2013. Frictional properties and microstructures of calcite-rich fault gouges sheared at subseismic sliding velocities. *Pure Appl. Geophys.* 1–24. <http://dx.doi.org/10.1007/s00024-013-0760-0>.
- Weeks, J.D., Tullis, T.E., 1985. Frictional sliding of dolomite: A variation in constitutive behavior. *J. Geophys. Res.* 90, 7821. <http://dx.doi.org/10.1029/JB090iB09p07821>.
- Wenk, H.-R., Shore, J., 1975. Preferred orientation in experimentally deformed dolomite. *Contrib. Mineral. Petrol.* 50, 115–126. <http://dx.doi.org/10.1007/BF00373331>.
- Wilkinson, M., Haszeldine, R.S., Fallick, A.E., Odling, N., Stoker, S.J., Gatloff, R.W., 2009. CO₂-mineral reaction in a natural analogue for CO₂ storage—implications for modeling. *J. Sediment. Res.* 79, 486–494. <http://dx.doi.org/10.2110/jsr.2009.052>.
- Zhang, X., Spiers, C.J., 2005. Compaction of granular calcite by pressure solution at room temperature and effects of pore fluid chemistry. *Int. J. Rock Mech. Min. Sci.* 42, 950–960.
- Zhang, X., Spiers, C.J., Peach, C.J., 2010. Compaction creep of wet granular calcite by pressure solution at 28°C to 150°C. *J. Geophys. Res.* 115, B09217. <http://dx.doi.org/10.1029/2008jb005853>.